



FINAL REPORT

OREGON
TRANSPORTATION
RESEARCH AND
EDUCATION CONSORTIUM

Laboratory Performance of Highway Bridge Girder Anchorages Under Simulated Hurricane-Induced Wave Loading

**OTREC-RR-12-05
July 2012**

**LABORATORY PERFORMANCE OF HIGHWAY
BRIDGE GIRDER ANCHORAGES UNDER
SIMULATED HURRICANE-INDUCED WAVE
LOADING**

Final Report

OTREC-RR-12-05

by

Jora Lehrman
Christopher Higgins, Ph.D., P.E.
Daniel Cox, Ph.D.

School of Civil and Construction Engineering
Oregon State University

for

Oregon Transportation Research
and Education Consortium (OTREC)
P.O. Box 751
Portland, OR 97207



OTREC
OREGON TRANSPORTATION RESEARCH
AND EDUCATION CONSORTIUM

July 2012

Technical Report Documentation Page			
1. Report No. OTREC-RR-12-05	2. Government Accession No.	3. Recipient's Catalog No.	
4. Title and Subtitle LABORATORY PERFORMANCE OF HIGHWAY BRIDGE GIRDER ANCHORAGES UNDER SIMULATED HURRICANE-INDUCED WAVE LOADING		5. Report Date July 2012	
		6. Performing Organization Code	
7. Author(s) Jora Lehrman Christopher Higgins, Ph.D., P.E. Daniel Cox, Ph.D.		8. Performing Organization Report No.	
9. Performing Organization Name and Address School of Civil and Construction Engineering 101 Kearney Hall Oregon State University Corvallis, OR 97331		10. Work Unit No. (trais)	
		11. Contract or Grant No. 2009-252	
12. Sponsoring Agency Name and Address Oregon Transportation Research and Education Consortium (OTREC) P.O. Box 751 Portland, Oregon 97207		13. Type of Report and Period Covered	
		14. Sponsoring Agency Code	
15. Supplementary Notes			
16. Abstract Many bridges along the Gulf Coast of the United States were damaged by recent hurricanes, and many more are susceptible to similar damage. This research examines the structural performance of common connection details used to anchor prestressed concrete girders to the substructure. Full-scale specimens were fabricated and tested under static and dynamic cyclic load histories. Dynamic load histories were developed from previously conducted hydraulic tests of a 1/5 scale model of a highway bridge under hurricane wave loads. The load effects considered included the pseudo-statically applied vertical uplift force, horizontal force, combined horizontal and vertical forces, and dynamically applied combined horizontal and vertical forces. This research describes the structural performance of the details under these loading conditions, provides improved understanding of connection performance, and enables better design details for new bridge construction and for rehabilitation of existing bridges to resist hurricane loads to produce surface transportation infrastructure that is more resilient to natural hazards.			
17. Key Words		18. Distribution Statement No restrictions. Copies available from OTREC: www.otrec.us	
19. Security Classification (of this report) Unclassified	20. Security Classification (of this page) Unclassified	21. No. of Pages 128	22. Price Price

ACKNOWLEDGEMENTS

This research was funded by Oregon Transportation Research and Education Consortium (OTREC) and the National Science Foundation with grant CMMI 0800822 of the Hazard Mitigation and Structural Engineering program. Dr. Keith Kaufman of Knife River in Harrisburg, OR, provided helpful suggestions and guidance during the fabrication of the specimens. Mr. Robbie Chambless of the Alabama Department of Transportation, Mr. Artur D'Andrea of the Louisiana Department of Transportation, and Mr. Rick Renna of the Florida Department of Transportation provided typical details of AASHTO III superstructure connections. The findings, conclusions and recommendations presented are those of the authors and do not necessarily reflect the views of the project sponsors or individuals acknowledged.

DISCLAIMER

The contents of this report reflect the views of the authors, who are solely responsible for the facts and the accuracy of the material and information presented herein. This document is disseminated under the sponsorship of the U.S. Department of Transportation University Transportation Centers Program in the interest of information exchange. The U.S. Government assumes no liability for the contents or use thereof. The contents do not necessarily reflect the official views of the U.S. Government. This report does not constitute a standard, specification, or regulation.

TABLE OF CONTENTS

ABSTRACT	1
1.0 INTRODUCTION	3
2.0 BACKGROUND	5
2.1 Padgett <i>et al.</i> (2008)	5
2.2 Chen <i>et al.</i> (2009)	6
2.3 Douglass <i>et al.</i> (2006)	6
2.4 Marin and Sheppard (2009)	7
2.5 AASHTO Guide Specifications for Bridges Vulnerable to Coastal Storms	8
2.6 Bradner (2008)	9
2.7 Schumacher <i>et al.</i> (2008)	9
2.8 Limitations of Knowledge	10
3.0 RESEARCH OBJECTIVES	11
4.0 EXPERIMENTAL DESIGN	13
4.1 Model Wave Force Data	13
4.2 Anchorage Selection	17
4.2.1 Threaded Insert/Clip Bolt Anchorage (CB)	18
4.2.2 Headed Stud Anchorage (HS)	19
4.2.3 Through Bolt Anchorage (TB)	20
4.3 Modifications to Girder and Details for Testing	20
4.4 Experimental Setup	24
4.4.1 Test Frame	24
4.4.2 Differences between Setup and In-Situ Conditions	27
5.0 EXPERIMENTAL TEST PLAN	29
5.1 Instrumentation	30
5.1.1 Strain Gages	30
5.1.2 Displacement Sensors	30
5.1.3 Load Cells	32
6.0 EXPERIMENTAL RESULTS	33
6.1 Data Processing	33
6.2 Series 1 Tests: Vertical Cyclic Loading	33
6.2.1 Test CB-1	34
6.2.2 Test HS-1	36
6.2.3 Test TB-1	38
6.3 Series 2 Tests: Horizontal Cyclic Loading	39
6.3.1 Test CB-2	40
6.3.2 Test HS-2	41
6.3.3 Test TB-2	42
6.4 Series 3 Test: Combined Horizontal and Vertical Cyclic Loading (pseudo-static)	44
6.4.1 Test CB-3	44
6.4.2 Test HS-3	46
6.4.3 Test TB-3	47
6.5 Series 4 Tests: Dynamic Loading	49
6.5.1 Test CB-4	49
6.5.2 Test HS-4	51
6.5.3 Test TB-4	54
7.0 DISCUSSION OF EXPERIMENTAL RESULTS	57

TABLE OF CONTENTS

7.1 Series Test: Isolated Vertical Loading	57
7.2 Series Test: Isolated Horizontal Loading	58
7.3 Series Test: Combined Psuedo-Static Horizontal and Vertical Loading.....	59
7.4 Series Test: Combined Dynamic Horizontal and Vertical Loading	60
7.5 Test Series Comparison.....	62
8.0 ANALYSIS	65
8.1 Comparison to AASHTO <i>Guide Specification</i>	65
8.2 Comparison to ACI 318-08	72
9.0 CONCLUSIONS	77
10.0 BIBLIOGRAPHY.....	79
APPENDICES	83
Appendix A: Self-Weight of Bridge Span	85
Appendix B: Instrumentation.....	87
Appendix C: Anchorage Details	93
Appendix D: Material Properties	97
Appendix E: ACI 318 Calculations.....	101
Appendix F: AASHTO Calculations	103
Appendix G: Specimen Production.....	111

LIST OF FIGURES

Figure 1: Example of damage at Escambia Bay, FL, after Hurricane Ivan (Courtesy W. Nickas).....	3
Figure 2: Replacement bridge at Biloxi Bay, MS (B. Hull, MDOT).....	4
Figure 3: Hydrodynamic 1/5-scale model of bridge span in wave flume (Bradner, 2008)	13
Figure 4: Instrumentation plan for Escambia Bay Bridge Model (Schumacher, 2009)	14
Figure 5: Comparison of command and feedback for vertical load forcing function using in-dynamic testing that shows elongation of the time scale used in testing.....	16
Figure 6: Typical AASHTO III dimensions	18
Figure 7: Reinforcing steel details at end of girder for Escambia Bay Bridge (from FDOT) ..	18
Figure 8: Anchorage details used in-situ by various transportation agencies: (a)Clip Bolt (b) Headed Stud, and (c) Through Bolt	19
Figure 9: Headed Stud (a) alternate FDOT detail (b) detail used in experiments	22
Figure 10: Specimen modifications required for testing	24
Figure 11: Laboratory setup.....	25
Figure 12: Schematic of laboratory setup.....	26
Figure 13: Connection plate for HS specimens	27
Figure 14: Typical instrumentation plan.....	31
Figure 15: Example specimen instrumentation	32
Figure 16: Strand slip instrumentation (a) CB Series, HS1-2 (b) HS3-4, TB specimens.....	32
Figure 17: Vertical load history for TB-1.....	34
Figure 18: Vertical load-deformation response for CB-1 (a), HS-1 (b), TB-1 (c).....	34
Figure 19: Cracking pattern specimen CB-1	35
Figure 20: Load vs. Strand slip for strand #9 CB-1	36
Figure 21: Failure of specimen HS-1.....	37
Figure 22: Cracking of specimen HS-1	38
Figure 23: Failure cracks in specimen TB-1.....	39
Figure 24: (a) Bridge response phases before and after failure of off-shore anchorages and (b) rotation due to lack of end diaphragm.....	40
Figure 25: Example of rotation of specimen HS-2	41
Figure 26: Horizontal load-deformation response for CB-2 (a), HS-2 (b), TB-2 (c)	42
Figure 27: Horizontal load v. Tilt for specimen TB-2	43
Figure 28: Horizontal load v. Strand slip for specimen TB-2.....	44
Figure 29: Horizontal load-deformation response for CB-3 (a), HS-3 (b), TB-3 (c)	45
Figure 30: Vertical load-deformation response for CB-3 (a), HS-3 (b), TB-3 (c).....	46
Figure 31: Cracking of specimen HS-3 due to bearing of flange on horizontal actuator loading plate	47
Figure 32: Horizontal load vs. Tilt for specimen TB-3	48
Figure 33: Initial cracking (a) and cracking at failure (b) for specimen TB-3.....	49
Figure 34: Example of command and feedback of applied vertical load history for specimen CB-4.....	50
Figure 35: Vertical load-deformation response for CB-4 (a), HS-4 (b), TB-4 (c) (Ultimate Test).....	51
Figure 36: Horizontal load-deformation response for CB-4 (a), HS-4 (b), TB-4 (c) (Ultimate Test).....	51
Figure 37: Vertical load-deformation response for CB-4 (a), HS-4 (b), TB-4 (c) (Initial Test)	52
Figure 38: Horizontal load-deformation response for CB-4 (a), HS-4 (b), TB-4 (c) (Initial Test)	52

LIST OF FIGURES

Figure 39: Example of command and feedback of applied vertical load history for HS-4 Real Time (a) and Half Time (b)	54
Figure 40: Example of command and feedback of applied vertical load history (a) and applied horizontal load history (b) for specimen TB-4 at 160% conditions with the original time scale.....	56
Figure 41: Observed cracking of specimen HS-4	61
Figure 42: Initial part of vertical load-vertical displacement behavior for specimen CB-1 showing softening	62
Figure 43: Assumed load distribution for typical bridge section assuming rigid superstructure.....	67
Figure 44: Maximum vertical load per anchorage - 12 anchor points used on the bridge.....	69
Figure 45: Associated horizontal force vs. maximum wave height for different numbers of anchor points and anchorage types	71

LIST OF APPENDIX FIGURES

1: Wave Conditions for Dynamic Loading	15
2: Loading Protocol.....	29
3: HS-4 Load Trials	53
4: Test Series Comparison – Initial Cracking	63
5: Test Series Comparison – Strand Slip	63
6: Test Series Comparison – Ultimate Capacity	64
7: Comparison of Input Parameters for AASHTO <i>Guide Specification</i>	65
8: Material Properties for ACI Calculations	72
9: CB Failure Modes.....	73
10: HS Failure Modes	74
11: TB Failure Modes	75
B- 1: CB-1 Instrumentation Plan	87
B- 2: CB-2 Instrumentation Plan	87
B- 3: CB-3 Instrumentation Plan	88
B- 4: CB-4 Instrumentation Plan	88
B- 5: TB-1 Instrumentation Plan.....	89
B- 6: TB-2 and TB-3 Instrumentation Plan	89
B- 7: TB-4 Instrumentation Plan.....	90
B- 8: HS-1 Instrumentation Plan.....	90
B- 9: HS-2, HS-3, and HS-4 Instrumentation Plan	91
C- 1: LADOT Misc. Span and Girder Details	93
C- 2: ALDOT Girder Details – Mobile Bay Crossing.....	94
C- 3: ALDOT Typical Details	94
C- 4: I-10 Escambia Bay Anchorage Details (FDOT).....	95
C- 5: F-5 Insert Technical Data.....	96
D- 1: Knife River Concrete Mix Data.....	97
D- 2: Headed Stud Stress/Strain Diagrams	98
D- 3: Mild Reinforcing Stress/Strain Diagrams.....	100
F- 1: Maximum Vertical Load per Anchorage for Four Anchorage Points	106
F- 2: AASHTO Vertical Load per Anchorage and Strand Slip - CB Anchorage	107
F- 3: AASHTO Vertical Load per Anchorage and Strand Slip – TB Anchorage.....	108
F- 4: AASHTO Horizontal Load per Anchorage and Strand Slip	108
F- 5: AASHTO Vertical Load per Anchorage and Crack Initiation	109
F- 6: AASHTO Horizontal Load per Anchorage and Crack Initiation.....	110
G- 1: Knife River Prestressing Bed.....	111
G- 2: Reinforcing Modifications to Test Specimens.....	112
G- 3: Top Flange Blockouts.....	113
G- 4: Clip Bolt (CB) Anchorage	114
G- 5: Headed Stud (HS) Anchorage	114
G- 6: Through Bolt (TB) Anchorage	115
G- 7: Torch Cutting of Prestressing Strand.....	116
G- 8: Removal of Specimen from Formwork	116

LIST OF APPENDIX FIGURES

ABSTRACT

Many bridges along the U.S. Gulf Coast were damaged by recent hurricanes, and many more are susceptible to similar damage. This research examines the structural performance of common connection details used to anchor prestressed concrete girders to the substructure. Full-scale specimens were fabricated and tested under static and dynamic cyclic load histories. Dynamic load histories were developed from previously conducted hydraulic tests of a 1/5-scale model of a highway bridge under hurricane wave loads. The load effects considered included the pseudo-statically applied vertical uplift force, horizontal force, combined horizontal and vertical forces, and dynamically applied combined horizontal and vertical forces. This research describes the structural performance of the details under these loading conditions, provides improved understanding of connection performance, and enables better design details for new bridge construction and rehabilitation of existing bridges to resist hurricane loads to produce surface transportation infrastructure that is more resilient to natural hazards.

1.0 INTRODUCTION

Recent strong hurricanes have caused significant damage to the transportation infrastructure along the U.S. Gulf Coast, shown in Figure 1. Hurricane Katrina caused over \$100 billion in total damage in 2005, with at least \$1 billion allocated to bridge repair and replacement (Padgett et al., 2008). Bridges are particularly critical assets as they limit the transportation system's capacity and can delay rescue, recovery and rebuilding efforts after an event. As the severity and frequency of Gulf Coast hurricanes may be expected to increase in the future, it is critical to identify bridges that are susceptible to damage and determine rehabilitating strategies so that bridges exhibit desired performance during these events.



Figure 1: Example of damage at Escambia Bay, FL, after Hurricane Ivan (Courtesy W. Nickas).

Since 2005, damaged bridge spans have been replaced by bridges with significantly higher superstructure elevations, shown in Figure 2. It is unlikely that future storm surges will be sufficiently high as to damage these new superstructures; however, the approach spans for

the new bridges may still be vulnerable. Additionally, there are many remaining low lying bridges throughout the Gulf Coast and Midatlantic that are susceptible to damage by future storm events.



Figure 2: Replacement bridge at Biloxi Bay, MS (B. Hull, MDOT).

Post-disaster surveys have shown that the damage to bridge superstructures was primarily caused by the elevated storm surge, which allowed larger waves to impact the structure (Douglass, 2006). The typical wave loads induced on the bridges, as well as the global failure modes, have been investigated. However, the behavior of the structural connection between the superstructure and substructure has not been previously examined.

2.0 BACKGROUND

The damage caused by recent hurricanes has raised awareness among the bridge engineering community about the vulnerability of coastal infrastructure to hurricane-induced wave loads. As a result, a number of post-disaster surveys were conducted to characterize the behavior of bridges and the failure modes associated with hurricane loading, as well as establish new design provisions to improve bridge performance for future events.

2.1 Padgett *et al.* (2008)

Padgett *et al.* (2008) quantified the damage patterns observed to bridges after hurricane Katrina. The damage was classified into five categories: damage due to surge-induced loading; impact damage; damage resulting from scour; damage due to water inundation; and wind damage. Surge-induced loading was characterized by the unseating of individual and multiple bridge spans at low elevation. The support connections of the individual spans had insufficient strength to resist the surge loads, and the wave forces pushed the spans off of the supports. These loads may have been intensified by the high wind loads on the bridges during the storm. In addition, impacts with barges, tug boats, oil drilling platforms, and other debris damaged piles, fascia girders, and caused span misalignment. Costs of repairing these bridges were estimated to be in the range of \$275 million for the replacement of US-90 to \$1,000 for minor repairs on moveable bridges.

2.2 Chen *et al.* (2009)

Chen *et al.* (2009) investigated the hydrodynamic conditions, magnitude of loading, and failure mode for three bridges damaged during Hurricane Katrina. To determine the hydrodynamic conditions, the authors utilized an advanced circulation model to determine the storm surge along the northeastern gulf of Mexico, and a third-generation spectral model to determine the coastal wave conditions. Using these models, the authors simulated the hydrodynamic conditions using the bathymetry and topography of the northern Gulf of Mexico. The models showed the maximum significant wave height as 3 meters along the US-90 Bridge at Bat St. Louis, LA, and 2.5 meters along the Biloxi Bay Bridge, AL. The models also allowed the authors to conclude that the primary cause of damage to the highway bridges was not the buoyant force of the bridges, but the surface waves impacting the bridge deck, as all bridges above the surge height but below the wave crests suffered damage. The authors quantified the magnitude of the wave loads using the methodology developed by McConnell (Chen *et al.*, 2009).

2.3 Douglass *et al.* (2006)

Douglass *et al.* (2006) reported the main failure mode of the decks to be caused by the wave loads. The storm surge brought the water level sufficiently high to allow the body of larger waves to strike the deck, causing the anchorages to fail. Subsequent waves would then push the unseated decks over and off of the pile caps. This report also features a new method presented as an interim guide to estimate the wave loads on coastal bridges. Using this method, the horizontal wave magnitudes range from 230 kips to 950 kips for each span, and vertical wave magnitudes range from 440 to 2,000 kips for each span, depending on the wave conditions and bathymetry of each site. The authors recommend constructing

bridges at a high enough elevation to avoid wave crests during a storm, and recommend more research to determine alternative design methods for vulnerable structures.

2.4 Marin and Sheppard (2009)

Marin and Sheppard (2009) discuss the development of a mathematical and computer model for wave loads on a bridge superstructure. Wave conditions in coastal areas are different from open ocean conditions where previous research efforts have been directed. The mathematical model is based on work originally presented by Morison (1950) and Kaplan (1992 and 1995). There are four general components that a structure undergoes from storm surge and wave loading: drag, inertia, buoyancy and slamming. The purpose of their study was to determine the inertia and drag coefficients in the model, as well as develop a predictive equation for wave-induced slamming forces (Marin and Sheppard, 2009). To apply the mathematical model, the authors developed a computer program called the Physics Based Model (PBM). The model works by calculating the water elevation, velocities, accelerations, and each component of the wave forces at each time step as a wave passes over the modeled bridge span.

To determine the inertia and drag coefficients for the model, physical tests were conducted at the University of Florida. A 1:8 scale model of the Escambia Bay Bridge superstructure was used along with four tri-directional load cells and three wave gauges to measure the loads on the structure and the wave conditions. The inertia and drag coefficients that produced the best least-squares fit to the test results were chosen.

The model was validated using hind-cast information about the storm conditions at Escambia Bay as input. The model predicts the performance of the bridge spans with air entrapment greater than 50% of the maximum possible for Hurricane Ivan.

2.5 AASHTO Guide Specifications for Bridges Vulnerable to Coastal Storms

The American Association of Highway and Transportation Officials (AASHTO) has recently developed a guide to calculate the loads on coastal bridges due to wave loading. The bridges can be designed for either the strength or extreme limit state, depending on the owner's assessment of the bridge and how quickly it must be utilized after an event. Three design cases are considered:

1. Maximum vertical force, including the vertical slamming force, with the associated horizontal force and the overturning moment at the trailing girder.
2. Maximum horizontal quasi-steady force, with the associated vertical force, including the vertical slamming force and the overturning moment at the trailing girder.
3. Prorated horizontal and vertical forces from cases 1 and 2 applied to the center of the exposed overhangs.

The equations are based on Kaplan's equations for offshore oil platforms. The PBM equations were developed at the University of Florida by Sheppard and Marin, and parameterized to account for the differences between a thin offshore platform in the open ocean and a much deeper bridge structure over a coastal waterway. The PBM was developed by calibrating a numerical model to match experimental data, and ran multiple simulations of different water and wave conditions. These simulations were then used to

modify the Kaplan equations. This design guide takes into account the type and size of the bridge span and girders, as well as the general bathymetry, characteristic wave heights, periods and attack angle. The guide also includes a trapped air factor (TAF) to account for air that can become entrained between the girders. If this trapped air cannot be vented, it will increase the buoyant or upward force on the bridge.

2.6 Bradner (2008)

Bradner experimentally measured the wave conditions and structural response of a 1:5 scale model of the I-10 Escambia Bay Bridge in Florida. Many of the individual bridge spans were unseated during Hurricane Ivan in 2004. An innovative laboratory setup was used that allowed the test specimen to move along the wave axis to simulate the dynamic response of the superstructure. Bradner found that the impact pressure, or slamming force of the wave, is not primarily responsible for the damage at the bent cap connections. The impact force is dissipated by the bridge superstructure.

2.7 Schumacher *et al.* (2008)

Schumacher *et al.* recorded data for loads on a bridge superstructure using a large scale model. The research was to compare the experimental results with analysis guides. Previous research regarding wave loads on structures has been limited to off-shore drilling platforms which differ from bridge superstructures. Wave conditions near off-shore platforms are different from coastal conditions, and off-shore platforms are always above the mean water level, whereas bridges can be submerged. Additionally, off-shore platforms are constructed using open-grid decks, which relieve vertical forces and force coupling effects. It was found that maximum loads in the vertical and horizontal directions do not

occur simultaneously, and the vertical load of the on-shore and off-shore girders differ, indicating the presence of an overturning moment.

2.8 LIMITATIONS OF KNOWLEDGE

All of the past research has been on developing analytical models and design specifications based on global bridge performance of reduced-scale hydraulic models. No research has been performed to investigate the performance of actual size bridge members or connections under hurricane-induced wave loading.

3.0 RESEARCH OBJECTIVES

The objectives of this study were to:

- Measure, for the first time in the field of ocean structural engineering, full-size structural connection-wave load response through hybrid testing.
- Quantify behavior of typical substructure-superstructure bridge connections under simulated hurricane-induced wave loading.
- Use experimental findings to enable owners to evaluate vulnerability of existing infrastructure to hurricane-induced wave loading.
- Report on the experimental findings to improve future anchor designs enabling performance enhancement of bridges under hurricane-induced wave loading.

4.0 EXPERIMENTAL DESIGN

The experiment was designed to isolate and then combine simulated hurricane-wave force components and applied laboratory specimens of representative full-size bridge superstructure to substructure connections. The approach relies upon a survey of design details from in-service bridges, previously generated wave-force data from a reduced-scale, a physical hydraulic model of a representative coastal bridge, representation of the load histories produced by hurricane-induced waves at the superstructure-to-substructure connections, and then application of these forces to full-scale connection specimens in the structural laboratory. These aspects and interactions are described subsequently.

4.1 Model Wave Force Data

Previous research performed at Oregon State University's O.H. Hinsdale Wave Research Laboratory large wave flume produced wave load response data on a 1:5 geometric scale based on the bridge geometry of I-10 over Escambia Bay, FL. A picture of the scaled span in the flume is shown in Figure 3.



Figure 3: Hydrodynamic 1/5-scale model of bridge span in wave flume (Bradner, 2008).

Data from over 400 tests of a scale model of a typical coastal prestressed girder bridge under a variety of wave conditions were developed in an earlier research study (Bradner, 2008). The tests were designed to be similar to a full-scale project using Froude scaling. Time history data was taken directly from the load cells placed in contact with the bridge model and the measurements were scaled to prototype scale (full-scale). For the horizontal load, it is assumed that all four anchorage points carry the load equally, so the horizontally oriented load cells (LC-1 and LC-2) were summed and divided by four. For the vertical uplift force, load cell (LC-3) on the seaward side of the bridge was used. See Figure 4 for the locations of the load cells.

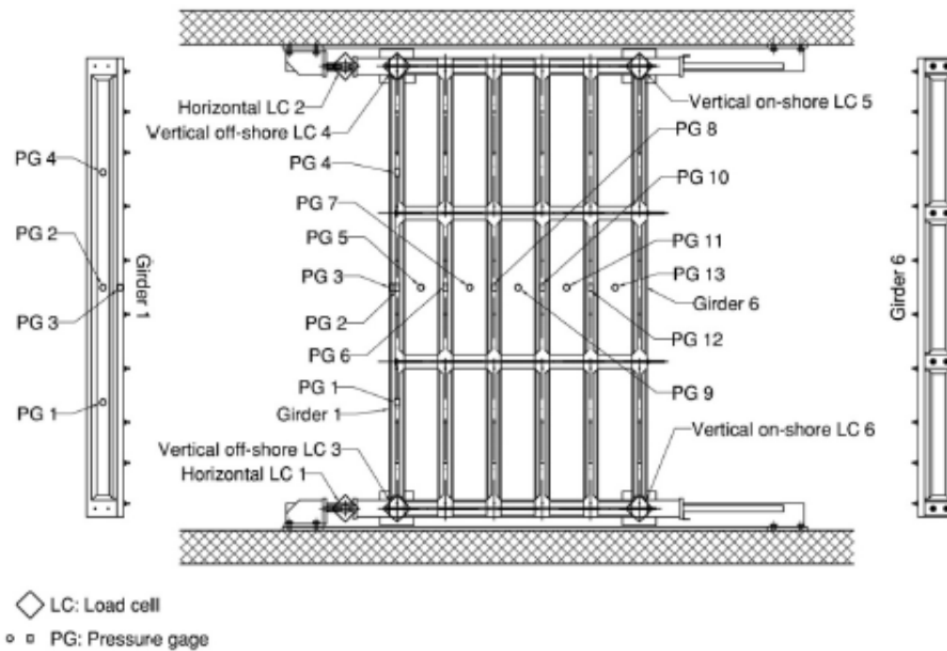


Figure 4: Instrumentation plan for Escambia Bay Bridge Model (Schumacher, 2009)

To scale Bradner's test data to full scale (using Froude scaling), time was multiplied by a factor of $\sqrt{5}$ and force was multiplied by 5^3 . Data were taken from trial reg1603, which had

conditions similar to Hurricane Katrina in Biloxi Bay, MS. The model and prototype values for wave height and frequency are listed in Table 1.

Table 1: Wave Conditions for Dynamic Loading

	<i>Wave Height m</i>	<i>Wave Period s</i>
Model	0.5	2.68
Prototype	2.5	5.99

The data were scaled to prototype scale and saved as a text file which was then read into a separate data acquisition system. That input file was read and converted to an analog output and used as the analog input command signal to the hydraulic controllers. The control signal was sent to the actuator and the actual applied force history was re-recorded in the data acquisition system along with the specimen responses. One of the challenges of this setup was to determine the rate to process the data so as to produce a loading time scale that closely matches the real-time loading history. It was found that with a time step of 0.001 seconds, the appropriate read rate was six data blocks at 1,000 Hz. Figure 5 shows an overlay of the scaled data from Bradner’s research and the load output from a typical test. If the specimen did not fail during the test, the time history loads were scaled higher and the test was re-run until the specimen failed. Amplitudes between the two signals remained excellent for individual wave cycles, particularly on the impact phase of the wave motion. The time scales were not as well correlated, as discussed later.

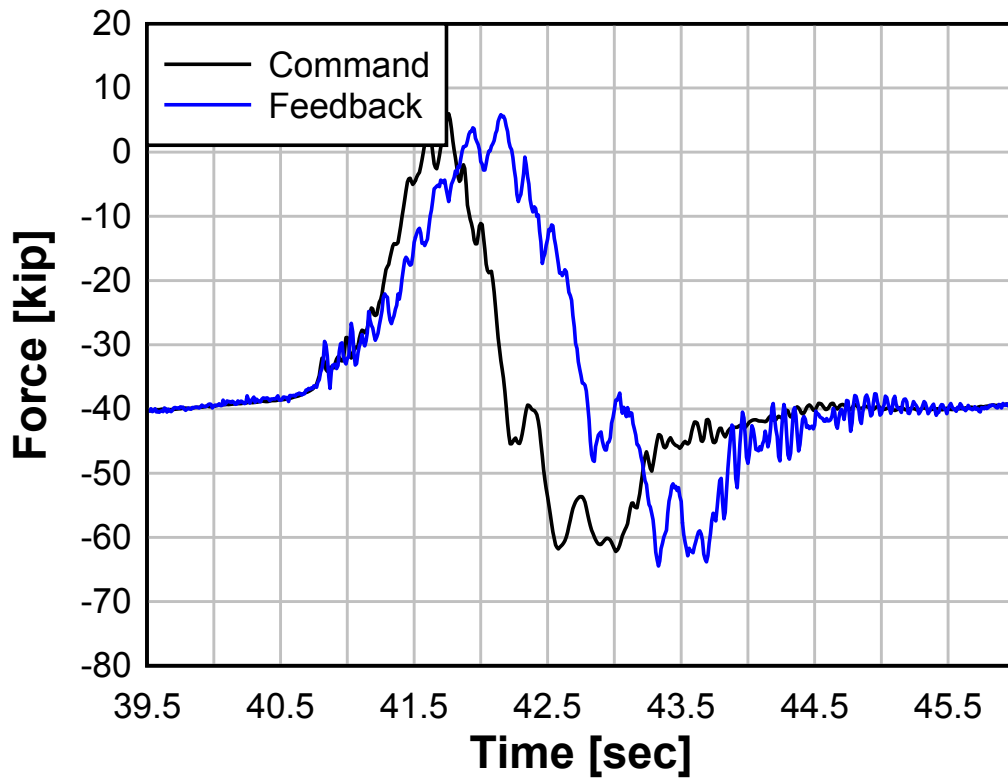


Figure 5: Comparison of command and feedback for vertical load forcing function using in-dynamic testing that shows elongation of the time scale used in testing.

For some of the test series, the flexibility of the connection and the limits of the hydraulic equipment prohibited the setup from matching the loads from the time history. The 30 gpm hydraulic power unit and the two 15 gpm servo-valves could supply enough hydraulic oil to compensate for the large deformations of the specimen, and the applied force from the actuator became limited to values lower than the target load. To accommodate this, the time history was stretched by a factor of two to slow the wave form and allow the hydraulics to meet load targets. This method of testing was the best representation of full-scale wave loads acting on a structural component within the limitations of the test setup.

4.2 Anchorage Selection

To determine the most commonly used anchorages in coastal infrastructure, a survey of state transportation agencies was conducted. Representatives from the Florida, Alabama and Louisiana DOTs were contacted and details were requested of the anchorages used on existing bridges that could be susceptible to hurricane loadings, or were damaged by past hurricanes. From this survey, three anchorage designs emerged as the most common and these were used in this study. The designs are discussed subsequently.

All of the connections are used to anchor AASHTO type-III bridge girders to the substructure cap beams. The prestressed girders have standardized dimensions as shown in Figure 6. This represents the full-scale girder size with the same proportions as that used in the reduced-scale study by Bradner (2008). The girders use prestressing and mild steel reinforcing, and the specimen details were selected to correspond to those detailed in the FDOT plans for the Escambia Bay Bridge. The plans called for two groups of prestressing strands:

1. (18) ½-in. diameter stress relieved straight strand pulled to 25,200 lbs each
2. (6) ½-in. diameter stress relieved double harped strand pulled to 25,200 lbs each.

The bursting steel stirrups consist of two L-shaped bars that extend the height of the girder and below the prestressing strand. Figure 7 shows the reinforcing details at the end of the girder.

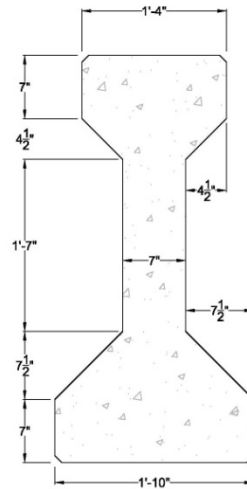


Figure 6: Typical AASHTO III dimensions.

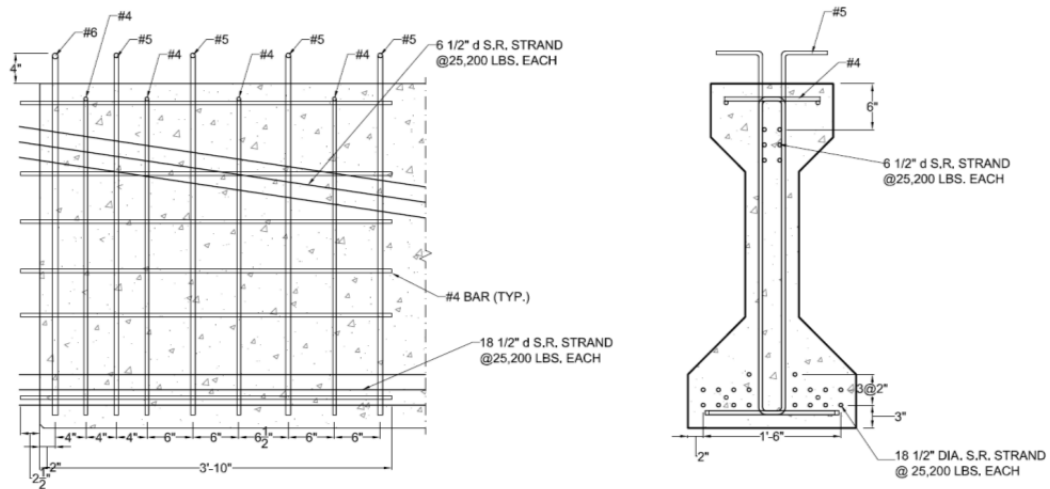


Figure 7: Reinforcing steel details at end of girder for Escambia Bay Bridge (from FDOT),

4.2.1 Threaded Insert/Clip Bolt Anchorage (CB)

The threaded insert (CB) detail was used in bridges in Alabama. Some of the bridges that used this detail were destroyed in Hurricane Katrina in 2005 (Padgett *et al.*, 2008). For this detail, the girders are cast with two 7/8-inch diameter threaded inserts on each side of the girder. During placement, the girders are connected to the pile cap using four 7/8-inch

diameter by 3-inch-long A325 bolts that thread into the inserts. An 8x6x1-inch steel angle connects the girder flange to the pile cap. The bearing pad produces a gap of approximately 1 inch between the bottom of the angle and the top of the pile cap. The inserts are located 5 inches apart in the longitudinal direction and are centered 8.5 inches from the edge of the specimen. The inserts are 4 inches above the bottom of the girder and placed between two rows of prestressing strand. A cross section of the detail is shown in Figure 8a.

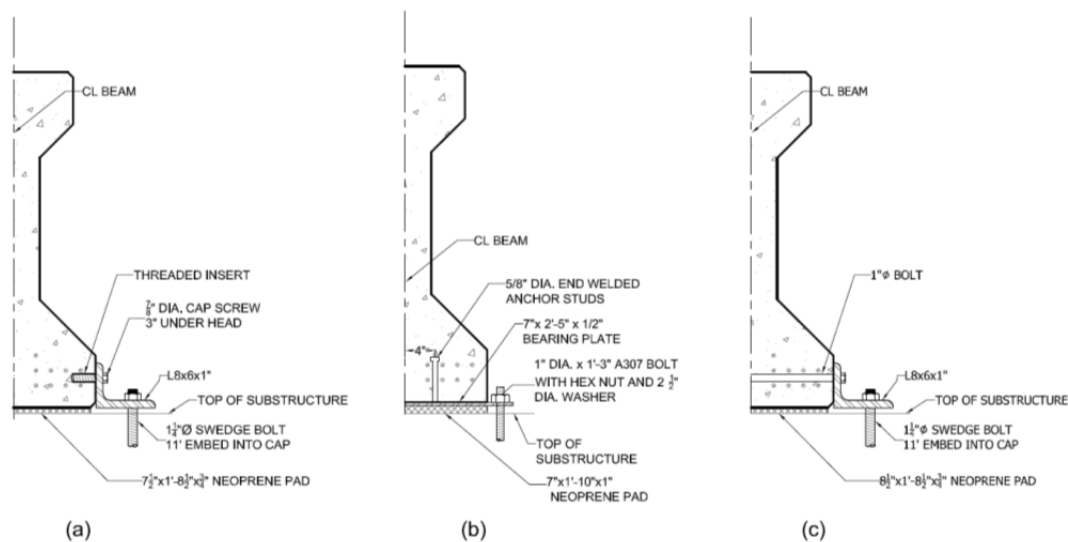


Figure 8: Anchorage details used in-situ by various transportation agencies: (a), Clip Bolt (b) Headed Stud, and (c) Through Bolt.

4.2.2 Headed Stud Anchorage (HS)

The headed stud anchorage (HS) detail was used on the Escambia Bay Bridge in Florida and some of these failed during Hurricane Ivan in 2004 (Douglass, 2004). The detail uses 4 5/8-inch diameter, 6-inch-long headed studs welded to a steel plate that extends past the flange section, where it is bolted to the pile cap with A 307 swedge bolts. The fabrication of this detail requires the precaster to slot the forms to allow the plate to extend beyond the cross section. In the case of Escambia Bay, only the exterior girders were detailed with this

anchorage. The studs were welded in an 8-inch by 5-inch rectangular pattern that was centered 8.5 inches from the edge of the beam. The plate rests on a 22x7x1-inch neoprene bearing pad. A cross section of the detail is shown in Figure 8b.

4.2.3 Through Bolt Anchorage (TB)

The through bolt anchorage (TB) is similar to the threaded insert except it passes completely through the bottom flange. This detail uses two 1-inch diameter bolts that pass through the bottom flange of the beam and connect to 8x6x1-inch angles that are bolted to the pile cap. The through bolts are spaced at 6 inches on-center and are located 8.5 inches from the edge of the beam and 4 inches from the bottom of the girder. This allows them to pass between two rows of prestressing strand. The bearing pad underneath the girder results in an approximately 1-inch-thick gap between the bottom of the connection angle and the top of the pile cap. A cross section of this anchorage is shown in Figure 8c. This detail is used for some bridges in Alabama. To date, bridges using this detail have not been exposed to extreme wave loading events, but are located in areas susceptible to future storms.

4.3 Modifications to Girder and Details for Testing

In order to conduct laboratory tests of bridge girder anchorages under simulated hurricane wave loading, a number of modifications were required as described subsequently. These modifications were made to facilitate testing of the anchorages while still representing as best as possible the existing conditions of the girders.

First, the harped prestressing strand was removed. The anchorages are not affected by the harped strand because the additional compression force is not fully developed in the section, and due to shear lag does not induce significant stresses at the anchorage locations.

Second, stress relieved strand is no longer readily available and low relaxation strand was used instead. The strand stress was the same as that used in the original design.

Third, for the connection types considered, the connection to the pile cap has been oversized to induce failure in the girder connections. The swedge and A307 bolts called for in the various DOTs were replaced with 1¼-inch diameter A325 bolts to ensure failure of the girder connection.

Fourth, the headed stud connection as detailed in the Florida DOT plans required the precaster to slot the forms to cast the ¼-inch thick plate integrally with the girder. That detail was not possible to construct for this study, so the anchorage was modified based on an alternate design in the Escambia Bay plans. The alternate design called for a 1¾-inch thick steel plate to be cast integrally with the concrete girder, which connected to a 1¼-inch thick plate with steel pintles, shown in Figure 9a.

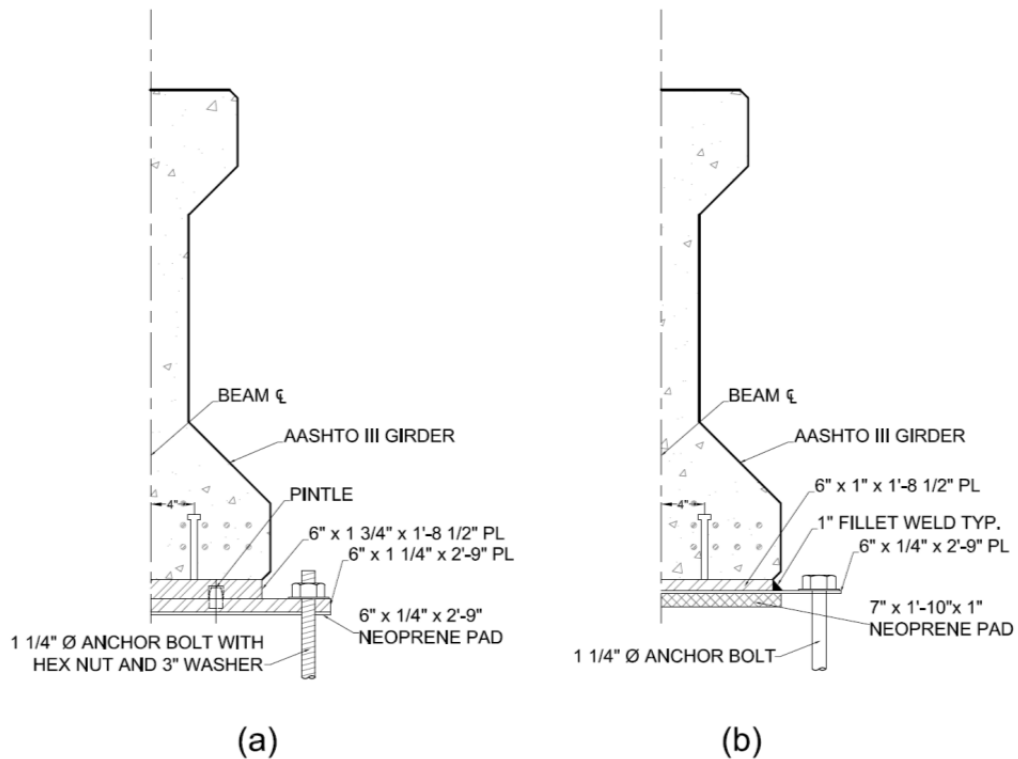


Figure 9: Headed Stud (a) alternate FDOT detail (b) used in experiments.

The detail constructed for this study is a hybrid of the detail constructed at Escambia Bay and the alternate design. It is characterized by a 1-inch thick steel plate welded to the headed studs and cast integrally with the girder, which is welded to a ¼-inch thick steel plate that extends beyond the width of the girder, as shown in Figure 9b. The plate thickness is not a factor in the observed failure mode of the anchorage.

Fifth, the length of the specimens was designed to allow each end of the specimen to be tested (two separate tests from each specimen - one on each end). The development length of the strand was conservatively assumed to be 3 feet, and the beam was designed to be 10 feet, or approximately three transfer lengths. If one side of the beam was damaged during a

test, there was a middle section of at least one transfer length to fully anchor the strand for the second test.

Finally, modifications were required to facilitate loading of the specimen, and to ensure a failure at the connection being examined. To apply vertical load, the specimen was fitted with a steel clevis that bolted through the stem of the AASHTO III girder. The top flange of the AASHTO section has been removed for the first 2 feet from the end of each side of the specimen to accommodate this loading fixture. A pre-assembled steel jig allowed the bolts to pass through the stem of the section, which was reinforced with additional #4 mild steel hairpins. Beyond the bursting steel, #6 stirrups are placed in the middle of the specimen to add strength and prevent damage to the midsection of the specimen. Additional #4 L-shaped bars were bundled with the first and last five stirrups and extended beyond the stem, but above the prestressing strand in the bottom flange. A U-shaped #4 bar was placed at the top of the stirrups to close the loop and ensure continuity between the separate L-shaped bars in the areas where the top flange was removed, shown in Figure 10. Additional pictures of specimen construction can be found in Appendix G.

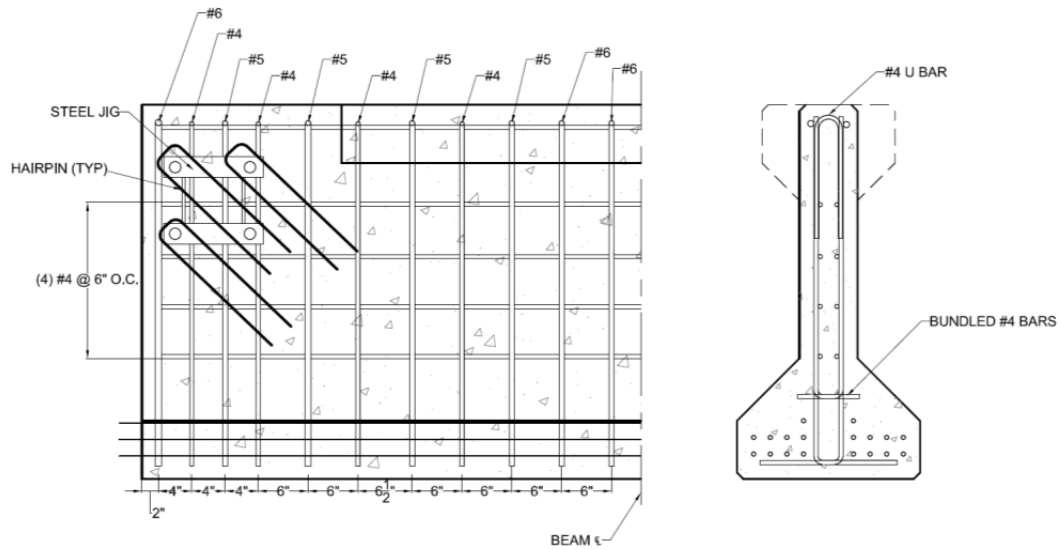


Figure 10: Specimen modifications required for testing.

4.4 Experimental Setup

Tests were carried out on the strong floor at the O.H. Hinsdale Wave Research Laboratory and the setup, instrumentation and test methodology are described in the subsequent sections.

4.4.1 Test Frame

The applied wave loads produce both vertical and horizontal force components on the connections. Thus, two actuators were required to impose the simulated wave load effects on the specimens. To accommodate these actuators, two separate reaction frames were needed.

Vertical Actuator

The vertical reaction frame was made up of two W12x120 steel frames spaced 4 feet on center. The frames supported a vertically oriented 500 kip hydraulic actuator that was

centered between the two frames. W12x120 columns were supported by two W14x159 stiffened steel beams 9 feet in length, which were anchored to the strong floor with 1¼-inch diameter high-strength threaded rods, shown in Figure 11.



Figure 11: Laboratory setup.

Horizontal Actuator

The horizontal reaction frame was made up of three steel sections. The first were 26 inches tall W12x120 stub columns with welded endplates anchored to the strong floor underneath the vertical reaction frame. This provided vertical clearance over the W14x159 frame supports. Connected to the top of the stub columns was a large, stiffened W21x150 which cantilevered over the stub columns on one side. This beam served as the pile cap to which the girder specimens were anchored. The pile cap was made of steel and not concrete, and was designed to ensure failure of the girder connections rather than the pile cap. To support the horizontal 500 kip actuator, a built-up section made of two W sections welded together and welded to a 2-inch thick end plate was bolted to the cantilevered end of the steel pile

cap, which reacts against the horizontal actuator in place. This frame was self reacting with the test specimen, minimizing secondary effects from the vertical load application. A schematic of the laboratory setup is shown in Figure 12.

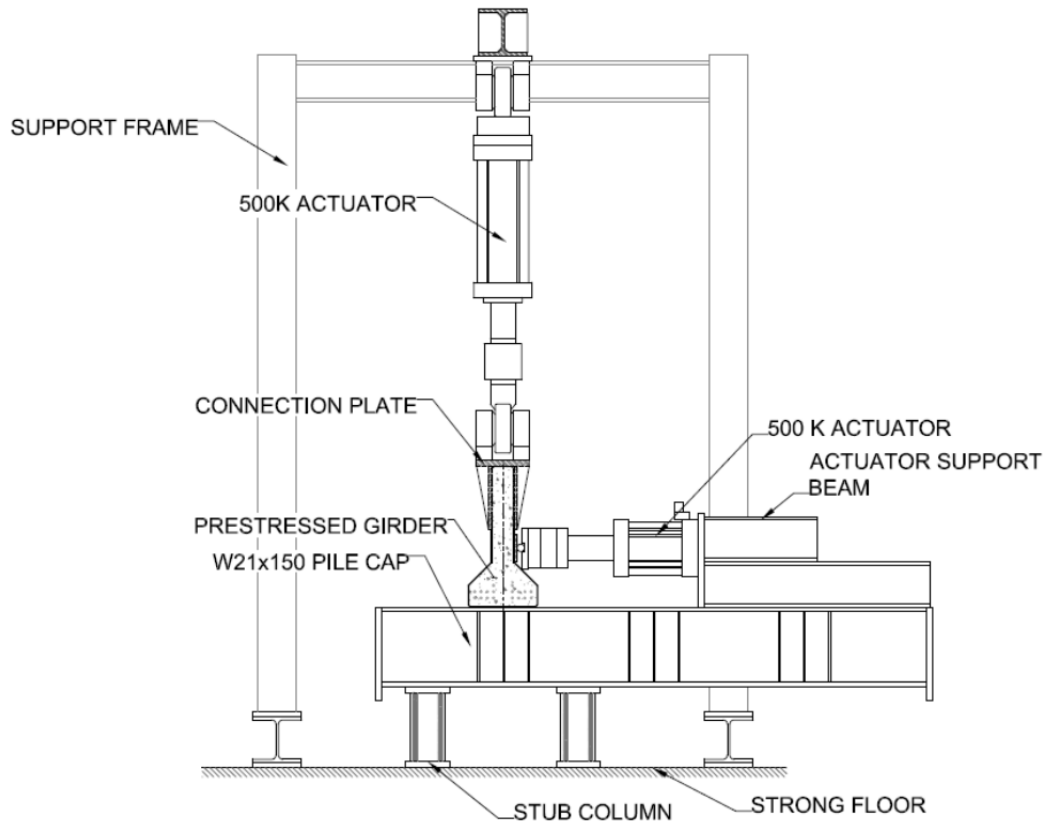


Figure 12: Schematic of laboratory setup.

Each test series required small modifications to the setup in order to anchor the connection. For the CB test series, 1.25-inch diameter holes were drilled at 5 inches on center directly onto the pile cap beam to match the hole pattern of the connection angles. The specimens for this series were bolted directly to the pile cap. Similarly, for the TB test series, 1.25-inch diameter holes were drilled at 6 inches on-center on the opposite side of the beam, requiring the setup to be rotated for this test series. For the HS test series, an additional

connection plate was required to connect the test specimen to the pile cap. The plate had holes to match the 5-inch hole pattern drilled through the pile cap, with an additional hole centered on the axis of the beam to allow a 1.25-inch diameter bolt to protrude up through the plate and connect to the specimen as seen in Figure 13.

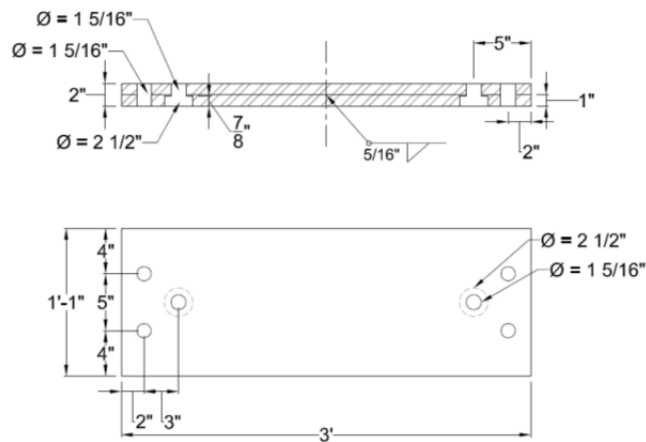


Figure 13: Connection plate for HS specimens.

4.4.2 Differences between Setup and In-Situ Conditions

The test setup described was designed to replicate in-situ conditions for bridge girders vulnerable to coastal storms. Some elements were not possible to recreate and are summarized in the following list:

- Supporting pile cap is constructed of steel instead of concrete.
- Horizontal load is applied slightly below the center of gravity of the diaphragm to prevent interference with the vertical loading plate.
- No concrete end diaphragm is present.
- No reinforced concrete deck is present.

- Self-weight of the superstructure is imposed on the anchorage by applying an initial downward force to the specimen with the vertical actuator.
- No corrosion damage or other environmental degradation exists.

5.0 EXPERIMENTAL TEST PLAN

There were four loading protocols used for each anchorage design, resulting in a total of 12 tests in the research program, as seen in Table 2. These tests were designed to isolate and then combine the force components that may cause damage to the connection, and whether the magnitude of load or the dynamic application of forces causes change in performance. Three of the test types were quasi-static cyclic, whereby the load was applied in increasing amplitude until specimen failure. The fourth test type was a dynamic load application with the applied loads (both horizontal and vertical) taken from reduced-scale hydraulic model tests and transformed to full-scale forces acting on the connections as described previously.

Table 2: Loading Protocol

<i>Series</i>	<i>Description</i>
1	Monotonic loading of vertical force component only.
2	Monotonic loading of horizontal force component only.
3	Monotonic loading of horizontal and vertical components simultaneously.
4	Real-time dynamic loading of horizontal and vertical components.

For test series 2, 3 and 4 a bridge self-weight load of 40 kips (negative) was imposed on the girder and regarded as the point of zero uplift. This initial applied force represents the tributary weight of components and wearing surface for the exterior girder at the support reaction. Test series 1 did not include the self-weight, as the vertical load must first overcome the self-weight before imposing demands in the connections.

5.1 Instrumentation

Instrumentation was deployed to measure the applied forces, and the specimen deformations and strains. A combination of strain gages, load cells, tilt sensors and displacement sensors were used to quantify the connection response. Data were recorded with a commercially available data acquisition system operating on a personal computer. Analog signals were converted to digital values, scaled to engineering units, displayed and then stored for later processing. Data was sampled at 5 Hz for pseudo-static tests, and 100 Hz for dynamic tests. Digital still photos and videos were taken of all tests.

5.1.1 Strain Gages

Strain gages are applied to the steel angles connecting the girders for both the through-bolt and threaded insert anchorages on both legs of the angle. Gages used were Vishay type CEA-06-125UN-120 measured to $1 \times 10^{-4} \mu\epsilon$. For tests series 1 and 2, only one angle was instrumented with twelve strain gages. Tests series 3 and 4 both angles were instrumented with six gages each. These gages record the bending strains of the angle under load. For the headed stud anchorages, strain gages are applied to the connection plate to measure plate bending.

5.1.2 Displacement Sensors

The deformations of the specimen were captured with BEI Duncan 9600 series displacement sensors, measured to 0.0001 inch. The displacement sensors measured displacement of the specimen relative to the pile cap, displacement of the angle relative to the pile cap, bolt displacement relative to the strong floor, and pile cap displacement

relative to the strong floor. See Figure 14 for the typical locations of the displacement sensors. Locations of displacement sensors for each test can be found in Appendix B.

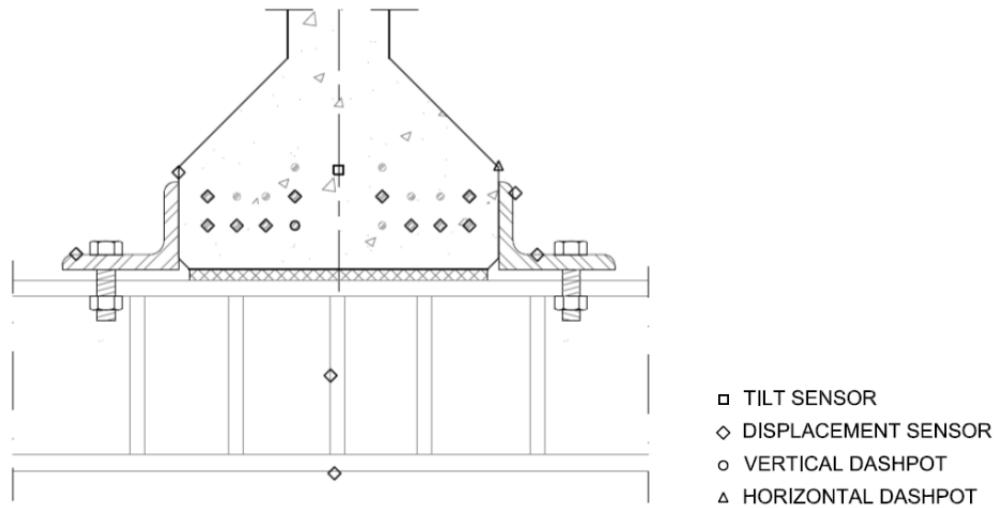


Figure 14: Typical instrumentation plan.

Strand Slip

Displacement sensors were used to measure the slip of selected strands in the specimens. To measure slip the sensors were attached to the exposed strand ends, which were cut so as to extend outside the concrete surface, shown in Figure 15. Figure 16 shows the location of these sensors for each test.



Figure 15: Example specimen instrumentation.

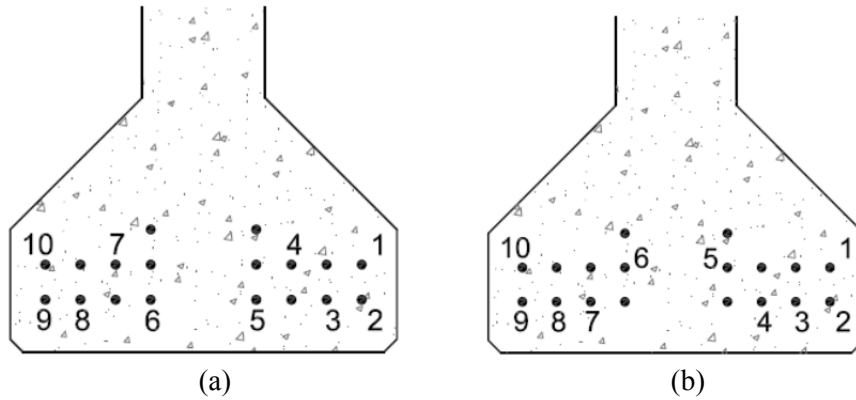


Figure 16: Strand slip instrumentation (a) CB Series, HS1-2 (b) HS3-4, TB specimens.

5.1.3 Load Cells

To determine the applied force to each anchorage, load cells were placed in-series to both the horizontal and vertical actuators. These load cells provided feedback for the hydraulic controller and were also recorded with the data acquisition system.

6.0 EXPERIMENTAL RESULTS

6.1 Data Processing

Recorded data were initialized to zero, and filtered to remove extraneous noise. Some displacement sensors reached the stroke capacity during some of the tests; data beyond the sensor maximum was disregarded. Test results are reported according to the loading protocol (Series 1, 2, 3 and 4) and then the specimen type (CB, TB and HS).

6.2 Series 1 Tests: Vertical Cyclic Loading

The clip bolt, headed stud and through bolt specimens were subjected to pseudo-statically increasing cyclic load amplitudes until failure of the specimen. A typical load history is shown in Figure 17. The load deformation responses for the three specimen types are shown in Figure 18. As seen here, the load deformation responses are shown at the same scale to highlight relative performance of the different connection types. Observed experimental responses for each of the specimens are described in this section.

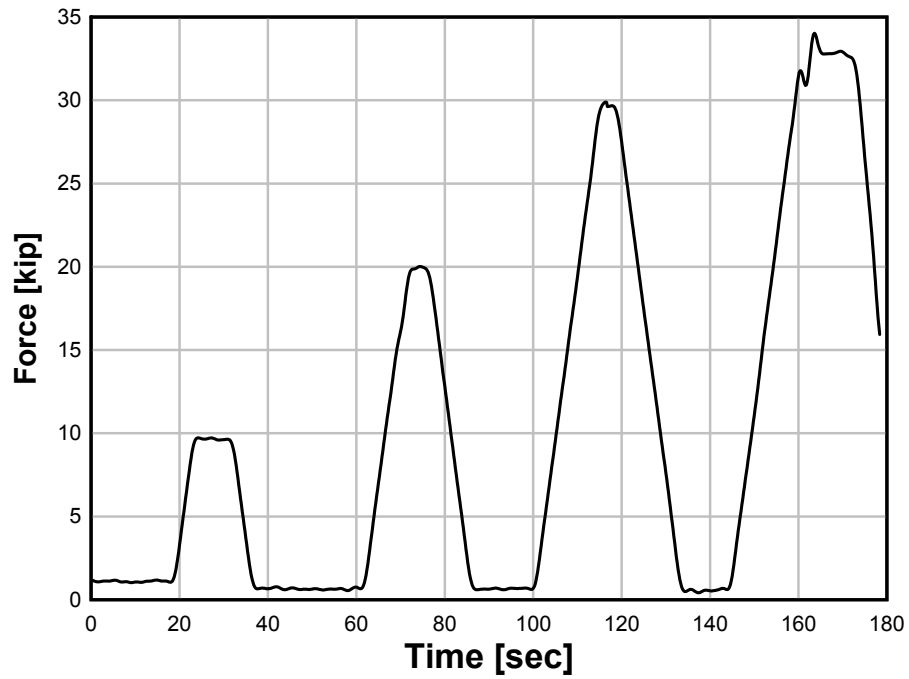


Figure 17: Vertical load history for TB-1.

6.2.1 Test CB-1

Figure 18a shows the load displacement behavior for CB-1. The specimen ultimately failed at a load of 23 kips. The failure was abrupt, with no visible cracking until the specimen ruptured around the inserts. Both sides did not fail simultaneously, one side failed and the other side failed on the next loading cycle.

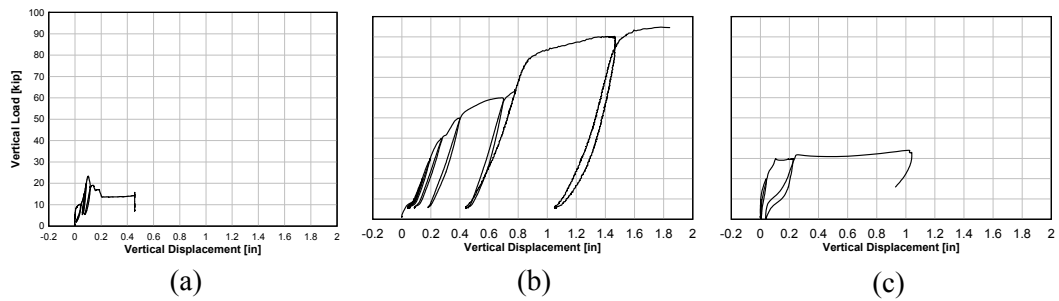


Figure 18: Vertical load-deformation response for CB-1 (a), HS-1 (b), TB-1 (c).

The failure plane of the anchorage is characterized by splitting of the concrete around the threaded inserts. The crack propagated at a 35° angle until reaching the edge of the flange, as shown in Figure 19.



Figure 19: Cracking pattern specimen CB-1.

At failure, the girder exhibited 0.11 inches vertical displacement. Post failure, the specimen exceeded the ½-inch stroke of the displacement sensors. The specimen displayed rigid body behavior, with no differential movement between the bottom flange bulb and the stem. There was a small amount of slip between the concrete girder and the steel connection angle.

Strand sensors 4, 5, 6 and 7 located near the center of the beam registered no slip throughout the test, even after failure. Sensors 3 and 8 registered minimal slip while exterior sensors 1, 2, 9, and 10 measured significant slip up to 0.15 inch before being

disrupted by the formation of cracks. Figure 20 shows the load versus strand slip of the specimen for strand 9. No yielding of the steel angles was measured.

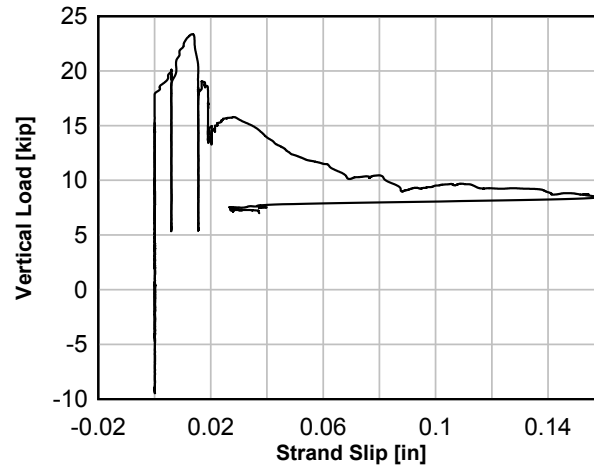


Figure 20: Load vs. Strand slip for strand #9 CB-1.

6.2.2 Test HS-1

The first attempt at this test resulted in failure of the fillet weld used to connect the embedded steel plate to the ¼-inch thick steel plate connected to the pile cap. Since the girders on the Escambia Bay bridge were constructed with only the ¼-inch plate that extended outboard of the girders, this failure was not compatible with field observations. The plates were re-welded with a larger fillet weld and the test was repeated on the same specimen.

The specimen failed at an applied vertical load of 94 kips. The connection was quite ductile, undergoing 1.84 inches of vertical displacement prior to failure. Figure 18b shows the load versus displacement response of the specimen. Failure of the specimen was categorized by yielding and fracture of the headed studs. The welded steel plates also yield and undergo large deformations prior to failure (as seen in Figure 21). These included

overall plate bending and local bearing at the bolt holes. Concrete cracking was observed around the corners of the embedded steel plate as seen in Figure 22, but no strand slip was measured by the instrumented strands, indicating that damage was localized and limited to the headed studs and concrete around the embed plate. The in-situ conditions at Escambia Bay used 1-inch diameter A307 swedge bolts in place of the 1¼-inch diameter A325 bolts used in the present experimental setup. The smaller and lower strength bolts used in the actual construction of the bridge were observed to have failed during Hurricane Ivan.



Figure 21: Failure of specimen HS-1.



Figure 22: Cracking of specimen HS-1.

6.2.3 Test TB-1

The specimen was loaded in tension in increments of 10 kips. The specimen failed at an applied vertical load of 34 kips tension. The load deformation response of the specimen is shown in Figure 18c. Starting at 15 kips, cracking of the concrete flange was observed prior to failure below the bottom layer of prestressing strand across the width of the girder flange. The concrete cracks propagated under the steel banding below the prestressing strand and mild steel. The test was stopped after the crack propagated across the width of the girder. Failure was categorized as tensile failure of the concrete surrounding the bolt holes, followed by bending of the bolts. Minimal rotation of the specimen was observed during the test. Maximum vertical displacement of the specimen was 1.02 inches at failure. No yielding of the steel angles was observed.



Figure 23: Failure cracks in specimen TB-1.

6.3 Series 2 Tests: Horizontal Cyclic Loading

For all the Series 2 tests, horizontal load was applied to the girder face at the web-flange transition location. This loading location (considered to be near the diaphragm location in the actual structure) causes both shear and a moment couple which induces tension and compression on opposite sides of the connection. The force couple causes the girders to rotate. On the actual bridges, the girders are connected to a concrete diaphragm, which restricts rotation of the individual girders, as represented in Figure 24. The diaphragm acts to convert the applied horizontal load into shear acting with net tension or compression at the connections rather than shear with bending of the connections. The laboratory-applied horizontal loading produces demands at the connection that are not fully representative of the in-situ condition of the bridge system when all anchorage points are in service. However, upon failure of the off-shore anchorages, the remaining anchorages are subjected to demands similar to the laboratory setup due to the rigid body rotation of the superstructure about the on-shore girder.

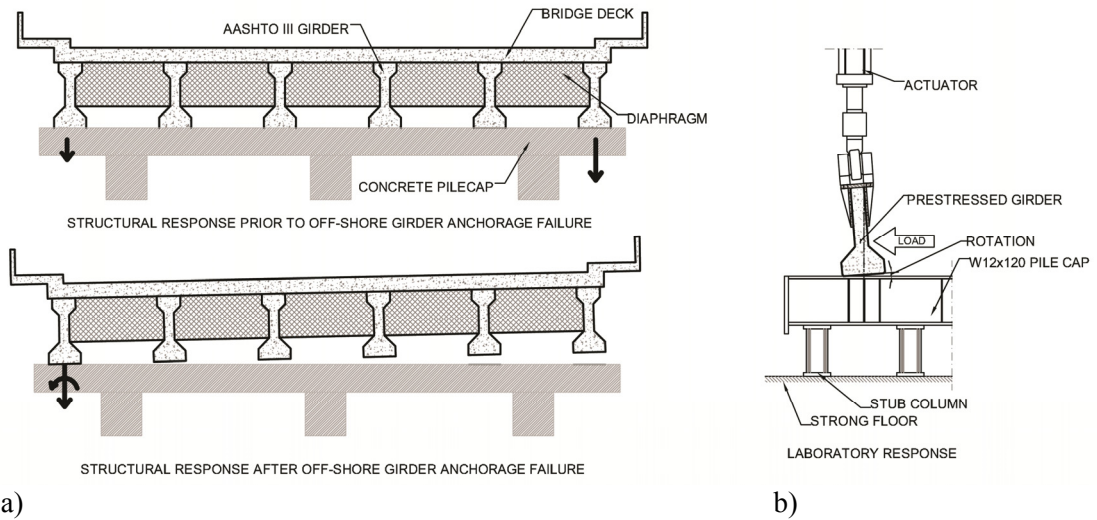


Figure 24: (a) Bridge response phases before and after failure of off-shore anchorages and (b) rotation due to lack of end diaphragm,

Due to the rotation induced on the isolated member specimens, both the HS and TB connection were not tested to failure, but the tests were halted when the rotation reached the limitations of the test setup. When sufficiently large specimen rotation occurred, the actuator clevis goes into bearing, creating an apparent increase in stiffness that is not representative of the connection. Despite these limitations, the test still serves as an indication of the overall horizontal and rotational performance of the connections and is a limitation of superstructure member-level tests.

6.3.1 Test CB-2

The response for this specimen was not recorded by the data acquisition system because the specimen failed during installation. During installation, the horizontal actuator failed the connection to the beam while trying to seat the horizontal bearing plate against the stem. The failure mode was similar to that of test CB-1, exhibiting cracking around the

threaded inserts and continuing at a 35° angle towards the bottom of the beam, exposing approximately 2 feet of the outermost strands. Only the loaded side of the beam was damaged, the side opposite of the actuator remained intact.

6.3.2 Test HS-2

The specimen was initially loaded with 40 kips of vertical pre-compression, and this was held constant throughout the test. This is representative of the dead weight of the bridge (attributed to the deck, diaphragms and guide rail) at this support location. The overall load-deformation response for specimen HS-2 is shown in Figure 26b. When the test was terminated due to excessive rotations, the studs had not failed. At higher load levels, the specimen exhibited large rotations that caused the studs to experience tension as well as shear forces. The apparent stiffening of the specimen at 50 kips was due to bearing of the actuator clevis at large relative rotations. Prying of the bolt on the tension side of the connection was observed, as well as yielding due to bearing of the bolt against the ¼-inch steel plate. No strand slip was observed during the test.

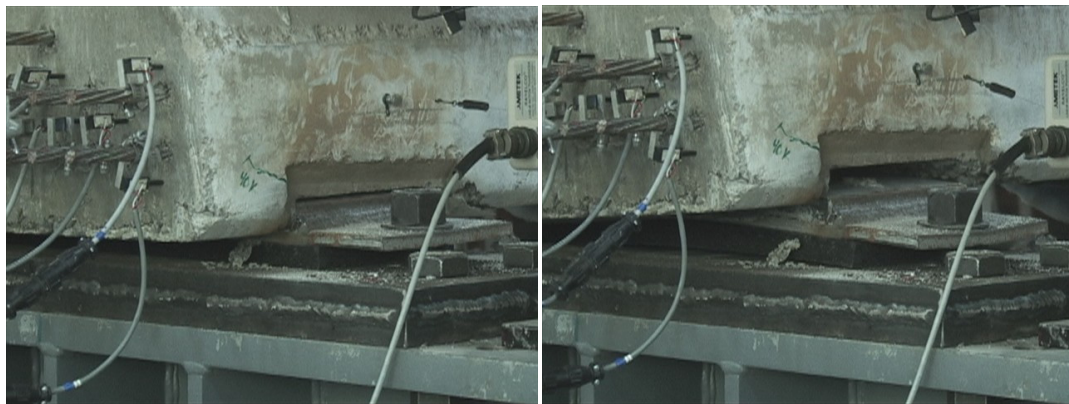


Figure 25: Example of rotation of specimen HS-2.

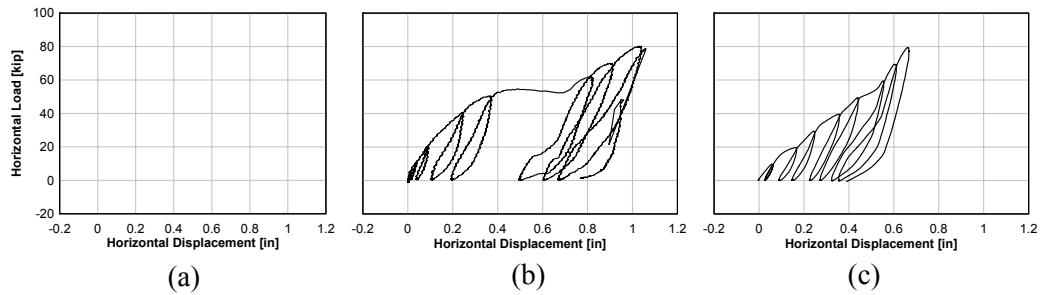


Figure 26: Horizontal load-deformation response for CB-2 (a), HS-2 (b), TB-2 (c).

6.3.3 Test TB-2

The specimen was initially vertically loaded with 40 kips of pre-compression, representing the dead load of the bridge at the support location. Then the horizontal loads were applied at increments of 10 kips. The vertical dead load was kept constant. The overall load-deformation response for specimen TB-2 is shown in Figure 26c. The maximum horizontal load was 80 kips when the test was terminated due to rotational limits of the setup. This is seen in Figure 26c as an apparent stiffening of the connection at approximately 60 kips. This was also observed in the load-rotation response of the specimen, as seen in Figure 27. The location of the load stiffening occurs at the rated rotational capacity of the actuator spherical bearing.

Prior to bearing of the actuator clevis, the specimen exhibited non-linear inelastic behavior and cracked at relatively low horizontal load. Cracking of the specimen was visible starting at 20 kips and propagated along six of the eight strands before the test was completed. The crack initiated at the through-bolt holes and propagated down towards the bottom layer of strand, and then continued below the strand, following around the banding steel. Similarly to test TB-1, when the specimen was removed from the test setup, the concrete spalled off exposing the strand, mild steel reinforcing and banding approximately 1 foot along the

length of the beam. All 10 displacement sensors measured strand slip during the test throughout the cross section of the girder. Strands 2 and 4 measured the largest slip of 0.221 inch and 0.107 inch, respectively. All other strands measured slip of less than 0.012 inch. Figure 28 shows the slip for strands 2 and 4 with respect to horizontal load. The data for strand 3 is disregarded due to a large piece of concrete spalling off near the gage.

Yielding of the steel angles was measured in strain gages 1 and 3-6. Only the angle on the loaded side of the specimen was instrumented. Maximum strain was 1,200 $\mu\epsilon$ measured by gage 6.

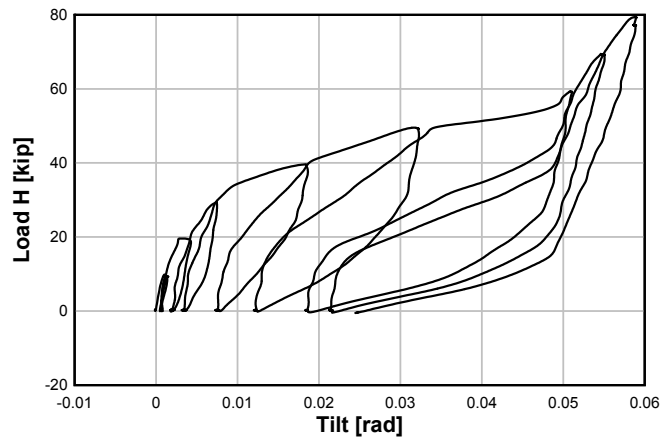


Figure 27: Horizontal load v. Tilt for specimen TB-2.

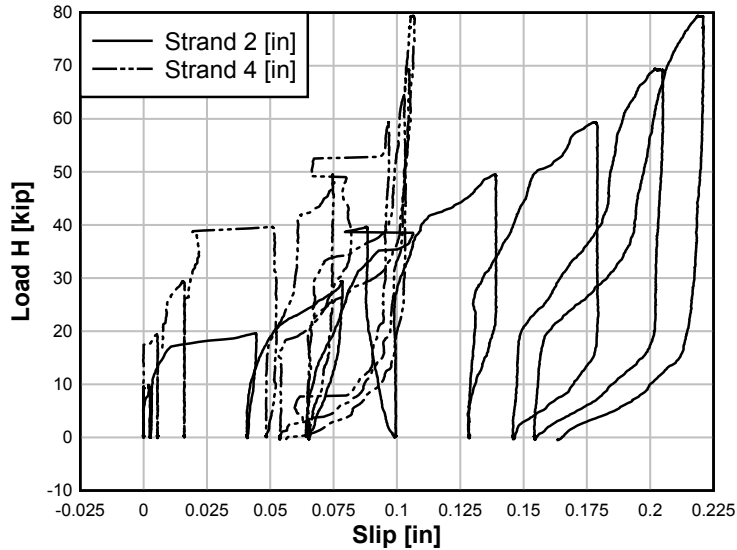


Figure 28: Horizontal load v. Strand slip for specimen TB-2.

6.4 Series 3 Test: Combined Horizontal and Vertical Cyclic Loading (pseudo-static)

For this test series, both vertical and horizontal loads were simultaneously applied to the specimen. The attributed dead weight of the bridge superstructure was applied to the test specimen, and vertical and horizontal loads were applied in a ratio of 2:1. The ratio of vertical to horizontal loading is based on the previously described reduced-scale model tests conducted by Bradner (2008). Similar to the Series 2 tests, these specimens also undergo rotations that are not fully characteristic of in-situ conditions, but this is somewhat mollified by the simultaneous application of the vertical loading.

6.4.1 Test CB-3

The overall load-deformation response for specimen CB-3 is shown in Figure 29a and Figure 30a for the horizontal and vertical directions, respectively. The specimen was initially loaded with 40 kips of vertical pre-compression representing the dead weight of

the bridge at this support location. The vertical load was decreased at increments of 5 kips (eventually becoming tensile), while a horizontal load component was simultaneously applied starting at zero and increasing at 2.5-kip increments. The ultimate failure load for this specimen was 3.81 kips of vertical tension and 19.19 kips of horizontal compression. There were minor cracks visible prior to failure; however, the failure was abrupt, as the threaded inserts ruptured from the side of the flange. The distress was similar to that observed for tests CB-1 and CB-2, with cracking around the threaded inserts and continuing to the bottom of the beam, exposing the prestressing strand. Only the off-shore side of the connection failed, while the unloaded side remained intact due to the horizontal load eccentricity. Strand slip was recorded in strands 1-4, located on the off-shore side of the beam. Maximum strand slip was seen in strand 2 with a magnitude of 0.051 inch. Yielding of the steel angles was recorded in strain gages 7-12, with the exception of gage 10 which failed during the test. These gages were located on the on-shore side of the specimen. Maximum strain was $1468 \mu\epsilon$, measured by gage 11 at failure.

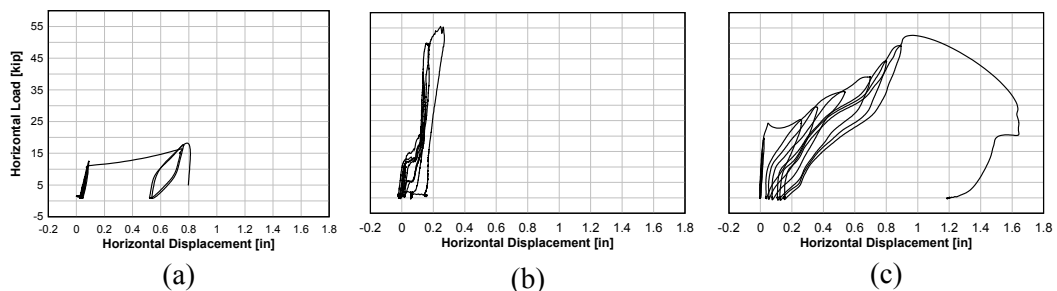


Figure 29: Horizontal load-deformation response for CB-3 (a), HS-3 (b), TB-3 (c).

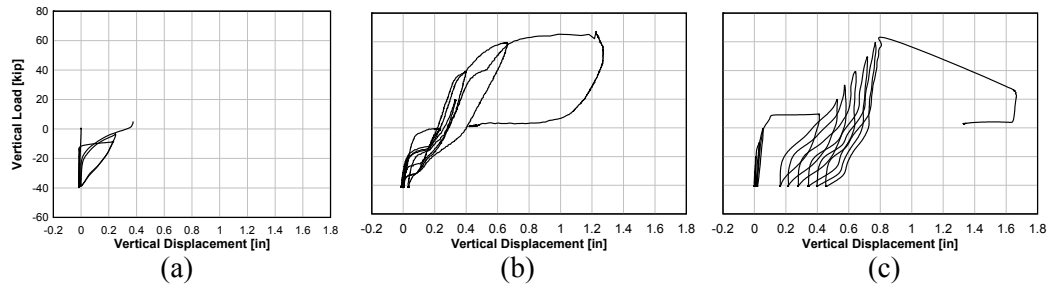


Figure 30: Vertical load-deformation response for CB-3 (a), HS-3 (b), TB-3 (c).

6.4.2 Test HS-3

The specimen was initially loaded with 40 kips of vertical pre-compression representing the dead weight of the bridge at this support location. Figure 29b and Figure 30b show the load-deformation response for test HS-3 in the horizontal and vertical directions, respectively. Behavior of this specimen was consistent with the results of HS-1 and HS-2. Large plastic deformations in the $\frac{1}{4}$ -inch connection plate, as well as prying of the bolts connecting to the pile cap, were visible prior the tension failure of the embedded headed studs. Ovalization of the bolt holes in the $\frac{1}{4}$ -inch plate was visible only on the off-shore side of the specimen. The specimen underwent 1.3 inches of vertical displacement prior to terminating the test. At 67.2 kips of vertical tension and 55.5 kips of horizontal load, the horizontal loading plate went into bearing against the bottom flange of the beam, cracking the concrete flange.



Figure 31: Cracking of specimen HS-3 due to bearing of flange on horizontal actuator loading plate.

6.4.3 Test TB-3

The specimen was initially loaded with 40 kips of vertical pre-compression representing the dead weight of the bridge at this support location. The vertical load was decreased in increments of 10 kips while a horizontal load component was simultaneously applied starting at zero and increasing at 5-kip increments. Figure 29c and Figure 30c show the load versus displacement behavior for TB-3 in the horizontal and vertical directions, respectively.

The failure of the connection was dominated by the vertical component of force, and is characterized by cracking in between the layers of strand across the entire cross section. It can be seen that significant cracking occurs after overcoming the dead load of the structure, and then there is a period of stiffening in the beam before it fails. This stiffening can be attributed to the through bolts resisting the load in bending while the cracks in the concrete

propagate to failure. After initial cracking, the specimen began to rotate as seen in Figure 32. The primary cracking of the beam began at the through bolts and extended down below the bottom layer of strand, following the banding. At failure, when the beam cracked completely across the cross section, the through bolts did not displace as much as the rest of the specimen, pulling down on the bottom layer of strand and causing a secondary crack to form. This exposed more of the prestressing strands, as well as the mild steel reinforcing to the stem of the girder. During the course of the test, sensors from strands 3, 4 and 7 were damaged, but slip was measured prior to damage. Strands 1,5,6 and 10, located on the upper layer of strand, measured less than 0.007 inch during the test. Yielding of the steel angle was measured by all six strain gages on the loaded side of the specimen. Maximum strain was 1,360 $\mu\epsilon$ measured by gages 4, 5 and 6.

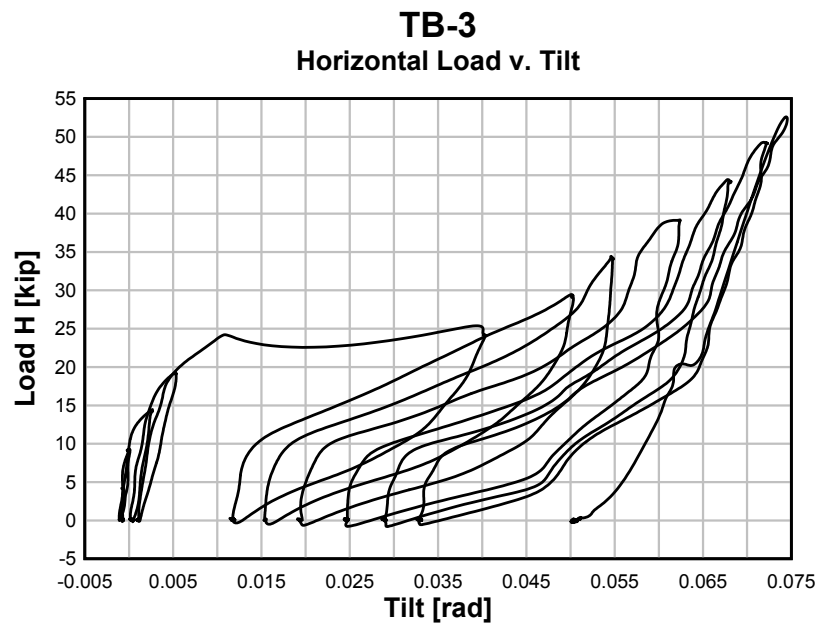


Figure 32: Horizontal load vs. Tilt for specimen TB-3,

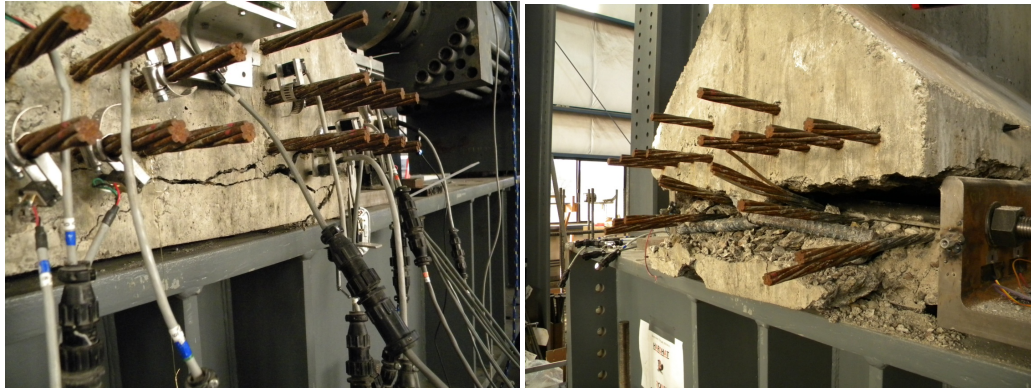


Figure 33: Initial cracking (a) and cracking at failure (b) for specimen TB-3.

6.5 Series 4 Tests: Dynamic Loading

For this test, load history data from load cells placed on the hydrodynamic scale model of the bridge superstructure in the wave flume were scaled up to full scale using Froude similitude. The values were discretized to 0.001-second time steps, and the digitized record was converted to an analog input using the data acquisition system to provide the control function to the two servo-hydraulic controllers used for the vertical and horizontal actuators. Each actuator then simultaneously applied the load history to the specimen. All specimens began the tests with an initial precompression of 40 kips to account for the bridge self-weight acting at the girder ends.

6.5.1 Test CB-4

The target and applied loading history for the vertical loading history are overlaid in Figure 34. As seen in this figure, some phase lag is found between the command and feedback, but the loading rate remains similar in the impact or initial loading phase of the waveform.

This was a limitation of the control and hydraulic flow capacity available in the structural laboratory.

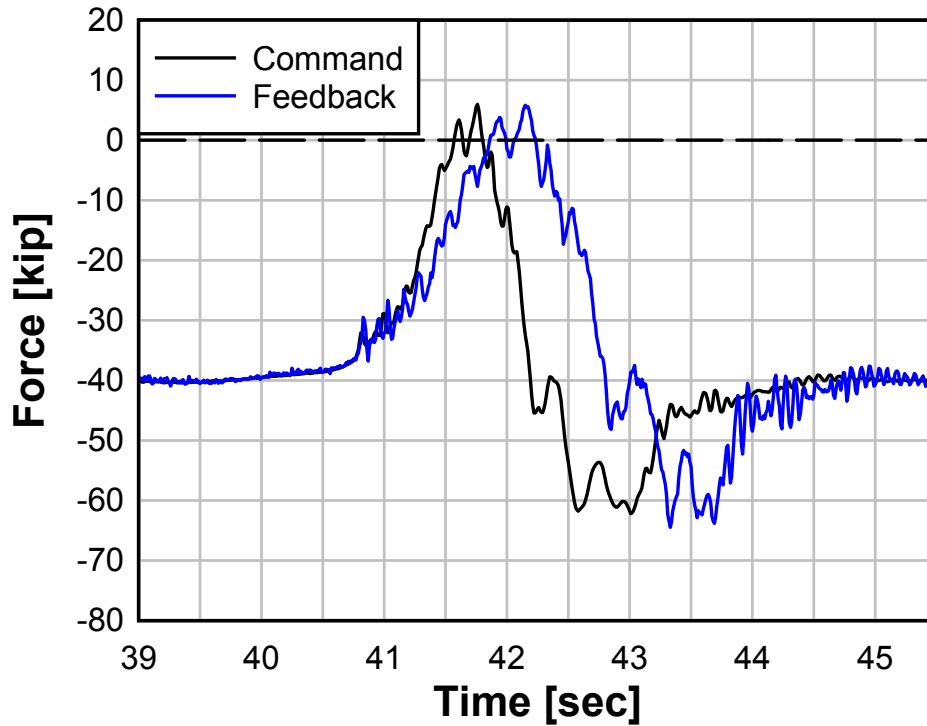


Figure 34: Example of command and feedback of applied vertical load history for specimen CB-4.

The specimen was loaded with 27 full waves with a period of approximately six seconds, and an uplift magnitude of 5 to 10 kips net tension (positive as shown in figures). The specimen cracked suddenly under the 25th wave, with the subsequent waves extending the cracks and severing the connection. Figure 35a and Figure 36a show the load deformation behavior of CB-4 for the vertical and horizontal responses, respectively. The specimen underwent less than 0.1 inch of vertical displacement, and 0.65 inch of horizontal

displacement. The specimen failed abruptly, with little cracking visible prior to failure. No yielding of the steel angles was measured.

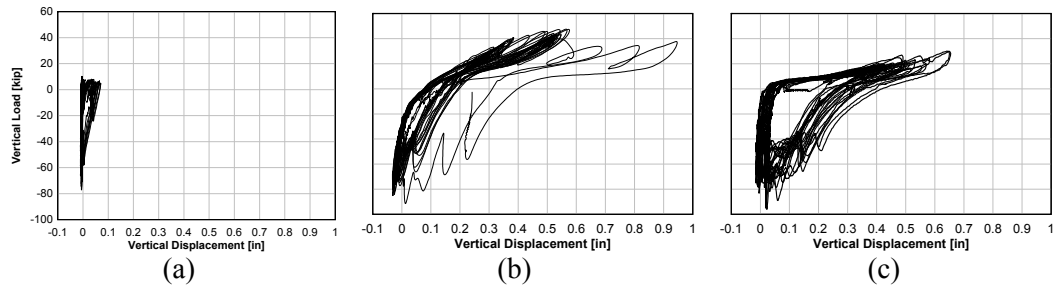


Figure 35: Vertical load-deformation response for CB-4 (a), HS-4 (b), TB-4 (c) (Ultimate Test).

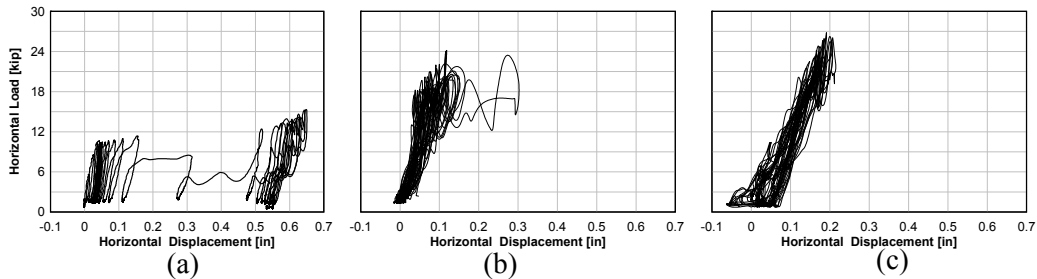


Figure 36: Horizontal load-deformation response for CB-4 (a), HS-4 (b), TB-4 (c) (Ultimate Test).

6.5.2 Test HS-4

The initial pre-compression load was applied to the specimen and then the horizontal and vertical loading history was applied. The initial test run of 100% Katrina conditions did not fail the specimen. The load-deformation behavior of the specimen during the initial test is shown in Figure 37b and Figure 38b for the vertical and horizontal responses, respectively. The test was then repeated with increasing load magnitudes. As described previously, the hydraulic actuators were unable to achieve the target load amplitudes due to limitations in

the hydraulic system, and the tests were repeated with the time scale stretched by a factor of two to achieve the prescribed load amplitudes. In the present specimen, failure was controlled by the steel studs, and this failure mode is not time dependent in this range of loading frequency and period. Table 3 shows the trials conducted on HS-4, the number of full-size waves, as well as the average maximum and minimum loads of those waves.

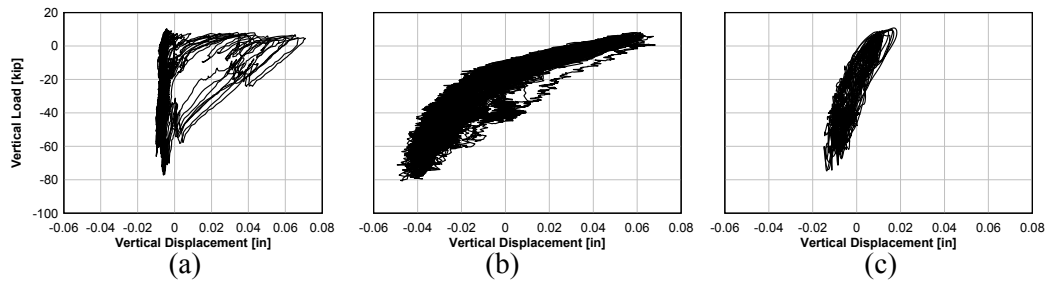


Figure 37: Vertical load-deformation response for CB-4 (a), HS-4 (b), TB-4 (c) (Initial Test).

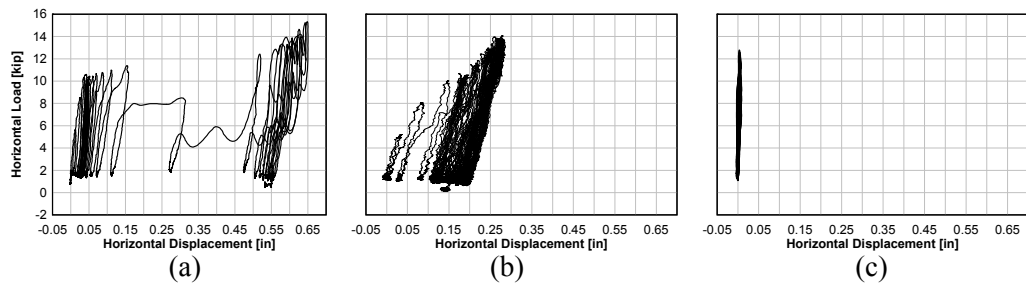


Figure 38: Horizontal load-deformation response for CB-4 (a), HS-4 (b), TB-4 (c) (Initial Test).

Table 3: HS-4 Load Trials

<i>Load Amplitude</i>	<i>Period Amplitude</i>	<i>Trial</i>	<i>Cycles</i>	<i>Avg min [kips]</i>	<i>Avg Max [kips]</i>	<i>SR [kips]</i>
100	1.0	1	53	-10	60	70
120	1.0	1	41	-12	75	87
140	1.0	1	50	-12	80	92
160	1.0	1	25	-12	71	83
180	1.0	1	6	-12	85	97
180-2	1.0	2	6	-12	75	87
180-3	1.0	3	21	-12	75	87
200	1.0	1	25	-12	75	87
100 -2	1.0	2	23	-10	60	70
120-2	1.0	2	25	-15	80	95
120	2.0	1	25	-20	65	85
140	2.0	1	25	-25	74	99
160	2.0	1	25	-33	79	112
180	2.0	1	23	-37	82	119
Total:			373			

The half-time load data correlated significantly better than the real-time data, as shown in Figure 39.

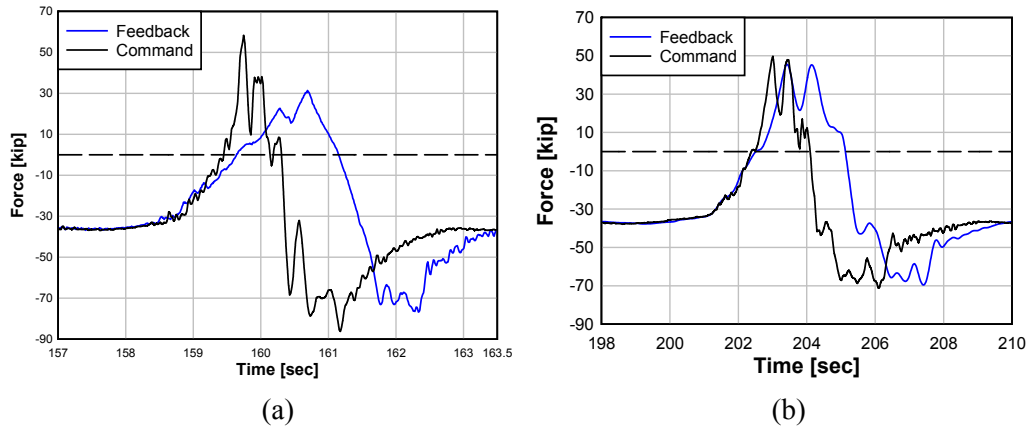


Figure 39: Example of command and feedback of applied vertical load history for HS-4 Real Time (a) and Half Time (b),

Similar to the other tests, failure of the connection was characterized by yielding of the connection plate, followed by yielding of embedded headed studs. Figure 35b and Figure 36b show the load versus displacement behavior for specimen HS-4 at failure. The specimen deformed 0.95 inch vertically prior to failure. The failure conditions represent a scaled response of over 180% for the Katrina event.

6.5.3 Test TB-4

The initial pre-compression load was applied to the specimen and then the horizontal and vertical loading history was applied. The specimen did not fail after the first trial at 100% of Hurricane Katrina conditions. It was found that the hydraulic actuators were again not able to achieve the prescribed load amplitudes. In order to fail the specimen, the timescale was stretched by a factor of 2 to allow the actuators sufficient time to achieve the tension load targets.

Some cracking of the specimen was visible with very little propagation during the initial test at 100% Katrina conditions at regular time. Figure 37c and Figure 38c show the load-deformation behavior for TB-4, for the vertical and horizontal responses, respectively. There was less than 0.009 radians of tilt measured, indicating that the actuator bearing did not exceed the available capacity. The maximum vertical deflection of the specimen was 0.018 inch; maximum horizontal deflection was 0.009 inch. Both figures show linear elastic behavior in both the vertical and horizontal directions for the duration of the test. Less than 0.005 inch of slip was detected during the trial, indicating no significant strand slip.

Correlation between the command and feedback load response at 160% of Katrina conditions using half-time scale undershot the vertical tensile load for each cycle, due to flow demands exceeding the flow capacity of the hydraulic system. While the compressive phase of the wave loading matched the 160% input values, the tensile loads achieved only 140% Katrina conditions.

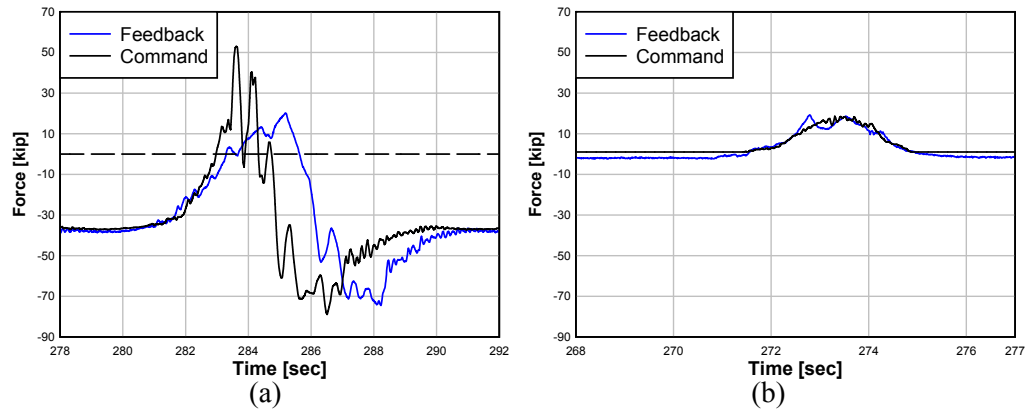


Figure 40: Example of command and feedback of applied vertical load history (a) and applied horizontal load history (b) for specimen TB-4 at 160% conditions with the original time scale,

Figure 35c and Figure 36c show the load deformation behavior of the specimen at ultimate capacity for the vertical and horizontal responses, respectively. Cracking of the specimen did not propagate across the entire section, but the specimen rotated sufficiently to bear against the spherical bearing on the vertical actuator. Yielding of the steel angles was measured in all 10 strain gages on both sides of the specimen. A maximum strain of $750 \mu\epsilon$ was recorded by gage 7, on the on-shore side of the specimen.

7.0 DISCUSSION OF EXPERIMENTAL RESULTS

Overall, the headed stud connection (HS) achieved higher load capacity and larger ductility compared with the other two connections considered. The HS series exhibited the least damage to the girder at failure, demonstrated by the lack of strand slip and concrete cracking. These imply improved long-term durability as chlorides cannot access the steel directly via cracks. Finally, as failure was controlled by yielding and fracture of the headed studs, the connection performance will be more predictable as compared to alternatives which rely on the concrete strength.

7.1 Series Test: Isolated Vertical Loading

The CB connection was the weakest of the three connection types in this type of loading, failing at a load of 23 kips. At failure, the concrete surrounding the inserts spalled off, exposing approximately 2 feet of the outermost strands. Girders could not be easily repaired as the entire connection had spalled from the girder, and a new connection point would have to be considered to re-use damaged spans. Corrosion of the strands would be an additional long-term concern, as the exposed strands and adjacent concrete cracking could transport chlorides along the length of the strand.

The TB connection performed slightly better than the CB connection, failing at 34 kips. However, the damage to the girder was much more extensive. The entire bottom layer of strands was exposed, and slip was measured on the second layer. Similar corrosion issues would be present with even more strands affected. The bottom of the girder at the

connection area would have to be completely reconstructed if the girders were to be salvaged.

The HS connection performed better than the TB and CB connections, failing at 90 kips. That was almost three times that of the TB connection and almost four times the load of the CB connection. The concrete exhibited superficial damage, with no strand slip observed. As currently designed, the connection would be difficult to repair, as the connection plate exhibited significant plastic deformations, and/or the headed studs would be fractured and require alternative connection of the girder to the bent cap. A key advantage of this connection is the predictability of the failure load as was controlled by the steel stud/plate properties. As a result, connections could be detailed to limit forces transmitted into the cap beam and substructure. This would preclude damage to components that would be more difficult and costly to repair or replace.

The HS connection is considerably more flexible than the TB and CB connections, which exhibited comparable stiffness until cracking occurs. The CB connection cracked before the TB connection and exhibited a smaller deflection prior to failure. The TB connection sustained larger deformations prior to the complete dislocation of the girder from the pile cap.

7.2 Series Test: Isolated Horizontal Loading

Due to the nature of the laboratory setup, the specimens underwent rotation during testing, creating force couple combined with the applied shear load. As the rotation of the specimen became sufficiently large, the vertical actuator clevis eventually went into

bearing, resulting in apparent load stiffening response of the connection. Tests were terminated when this was observed.

The CB connection failed while attempting to seat the bearing plate against the stem of the girder. The failure load for the specimen was not recorded, although the failure load was similar to that observed for the vertical load test on the seaward side of the connection. The HS load specimen was loaded to 80 kips prior to reaching the rotational limits of the setup. Plastic deformations of the plate and prying of the anchor bolt were noticeable, and no strand slip was recorded. The TB anchorage was also loaded to 80 kips before exceeding the rotational limits of the setup. Cracking throughout the cross section of the specimen was visible, and strand slip was measured throughout the cross section.

7.3 Series Test: Combined Psuedo-Static Horizontal and Vertical Loading

Similarly to the Series 2 test, the TB and HS connections exhibited large rotational deformations and the tests were stopped when the vertical actuator clevis went into bearing. The CB connection exhibited the lowest capacity, failing at 17 kips of horizontal load and 3 kips of vertical tension (essentially when the weight of the structure was overcome). The CB connection also underwent the smallest deformations of any of the connections. Damage to the connection on the seaward side was similar to the Series 1 test, with the outermost strands exposed along the length of the girder for a distance of 2 feet and the connection inserts were pulled from the girder flange.

7.4 Series Test: Combined Dynamic Horizontal and Vertical Loading

Specimens were initially subjected to 100% Katrina wave conditions. If the specimen did not fail at 100%, the intensity of the wave force magnitudes was increased in 20% increments until failure was achieved. Due to limitations of the hydraulic system, as well as the flexibility of the connections, the actuators were not able to achieve target load values at higher load levels. To compensate, the timescale was stretched by a factor of two to allow the actuators to better match the amplitude of the waveforms. For the HS connection, the failure was dominated by the steel studs, which do not exhibit time-dependent effects in the loading rate considered. For the TB connection, the failure was dominated by cracking of the concrete. By slowing the timescale, the strength of the connection is expected to be diminished slightly, as the slight increase in strength attributed to the concrete at higher loading rates is not fully captured in these tests.

The CB connection failed at the lowest load during the 100% Katrina conditions. The damage sustained by the connection was similar to that of the isolated and statically combined loading tests, with cracking around the inserts followed by spalling of the concrete around the inserts. This exposed the outermost prestressing strands along the transfer length. In this test, only the seaward side of the connection failed, subsequent wave loads caused the specimen to rotate, but did not cause failure on the on-shore side.

The TB connection demonstrated higher strength than the CB connection, ultimately failing at 160% of Katrina conditions. The damage sustained by the girder was much more extensive than the CB connection. The girder was cracked across the width of the cross section following along the prestressing banding. Once that crack propagated across the

entire flange width, a new crack around the bottom layer of prestressing appeared, holding the bottom layer of strand down and pulling it away from the rest of the girder as the wave uplift was applied. Cracking of the girder was observed at 100% Katrina conditions, making the strand susceptible to corrosion after this storm event.

The HS connection exhibited the highest strength, failing at 180% of Katrina conditions. Failure of the connection was similar to the isolated and combined pseudo-static tests and was characterized by tensile failure of the steel headed studs, and large plastic deformations of the connection plate. The damage to the concrete was limited to cracking around the reentrant corners of the plate interface. The HS connection was observed to fail during Hurricane Ivan, which had similar - if not less severe - wave conditions.

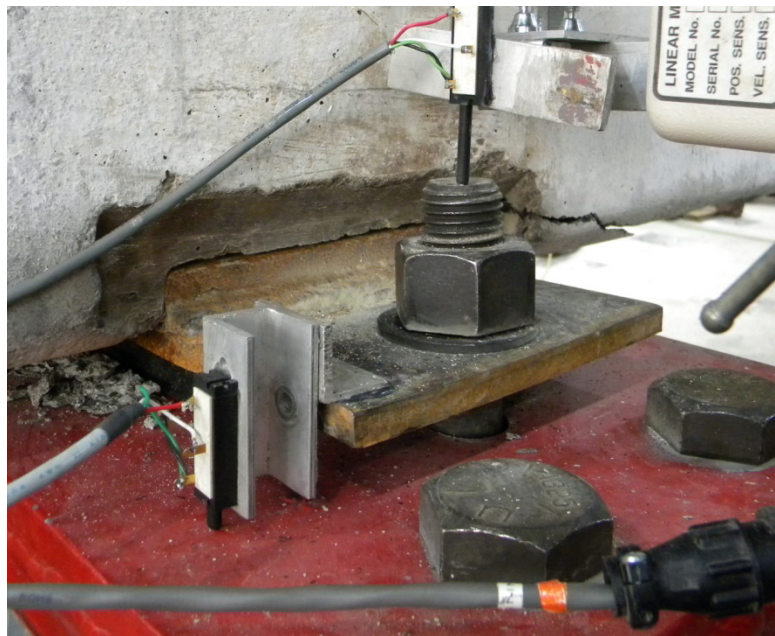


Figure 41: Observed cracking of specimen HS-4.

7.5 Test Series Comparison

Table 4 compares the cracking loads for each anchorage and test type. Cracking is defined as the point where the stiffness decreases on the load deformation plots. A range of loads is given for plots where the exact load at initiation of softening is unknown. Figure 42 shows an example of softening. The HS anchorage only exhibited superficial cracking during testing; the loads recorded in Table 4 indicate when the steel plate begins to separate from the concrete, allowing the specimen to rotate. For the CB anchorage, the horizontal cracking load was similar in the series 3 and series 4 test at 10.7 kips and 10.2 kips, respectively. The cracking load in the vertical direction for the series 3 and series 4 tests was not similar, ranging from -12.9 kips (compressive) in series 3 to approximately 8.3 kips (tensile) in series 4. For the HS anchorage, the horizontal cracking load was similar for the series 3 and series 4 tests, and the vertical load was similar for both tests. The TB anchorage showed no correlation in cracking load between the series 3 and series 4 tests.

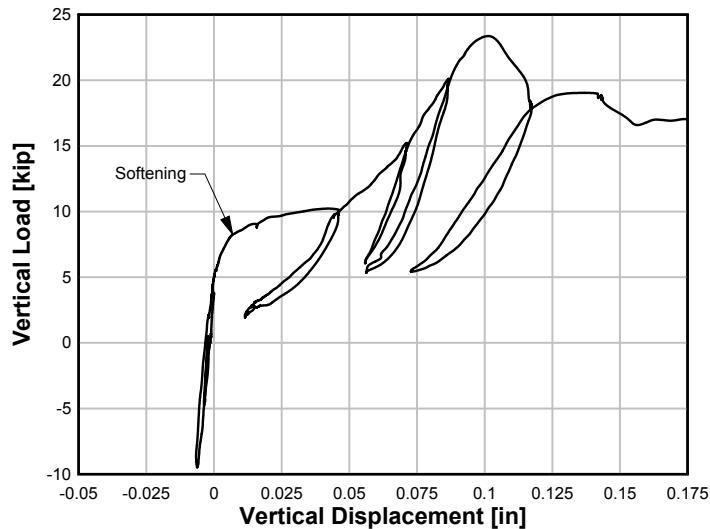


Figure 42: Initial part of vertical load-vertical displacement behavior for specimen CB-1 showing softening.

Table 4: Test Series Comparison – Initial Cracking

<i>Anchorage</i>	<i>Series 1</i> <i>V</i>	<i>Series 2</i> <i>H</i>	<i>Series 3</i> <i>V</i>	<i>Series 3</i> <i>H</i>	<i>Series 4</i> <i>V</i>	<i>Series 4</i> <i>H</i>
CB	8.1 k	-	-12.9 k	10.7 k	8.3±2 k	10.2±1 k
HS	40.8 k	51.6 k	-6.7±2 k	11.2±1 k	-13.9±5 k	10.3±2 k
TB	12.8±2 k	9.3 k	-16.2±1 k	20.0±0.5 k	0.0±2.5 k	5.0±2 k

The load at which strand slip was observed for each specimen is shown in Table 5 for each test. Strand slip affects the performance of the girder under service loads and has long-term performance concerns related to corrosion of the strand. No strand slip was measured for the HS anchorage in any of the four test series. For the CB anchorage, the horizontal load that induced strand slip was similar in the series 3 and series 4 tests, while the vertical load varied significantly in the different test series. Similarly, for the TB anchorage, the horizontal load that induced strand slip varied from 7 kips to 8.6 kips, while the vertical load varied from -33.6 kips (compressive) to 24.6 kips (tensile).

Table 5: Test Series Comparison – Strand Slip

<i>Anchorage</i>	<i>Series 1</i> <i>V</i>	<i>Series 2</i> <i>H</i>	<i>Series 3</i> <i>V</i>	<i>Series 3</i> <i>H</i>	<i>Series 4</i> <i>V</i>	<i>Series 4</i> <i>H</i>
CB	13.3 k	-	-28.2 k	5.7 k	-1.3 k	4.4 k
HS	N/A	N/A	N/A	N/A	N/A	N/A
TB	24.6 k	7 k	-33.6 k	7.1 k	8.1 k	8.6 k

The ultimate loads for each anchorage in each test series are shown in Table 6. The series 1 test demonstrated the anchorage capacity while all anchorages on a bridge are in service, and the wave loads cause vertical uplift without rotation. The series 3 test demonstrated the anchorage capacity after the off-shore anchorages fail, and the bridge cross section is able to rotate. The capacity of the remaining anchorages after the off-shore anchorages fail is diminished as compared to when all are intact. The capacity of the anchorages changed depending on the test type. The CB and HS anchorages resisted higher load in the series 1 (pseudo-static) than in the series 4 (dynamic) tests. The TB anchorage resisted higher loads under the series 3 (combined loading) test than under the series 1 (vertical load only) test due to the clamping effect of the force couple on the on-shore side of the flange.

Table 6: Test Series Comparison – Ultimate Capacity

<i>Anchorage</i>	<i>Series 1</i> <i>V</i>	<i>Series 2</i> <i>H</i>	<i>Series 3</i> <i>V</i>	<i>Series 3</i> <i>H</i>	<i>Series 4</i> <i>V</i>	<i>Series 4</i> <i>H</i>
CB	23 k	-	3.8 k	19.2 k	10 k	15 k
HS	94 k	80 k *	67.2 k *	55.5 k *	40 k	24 k
TB	34 k	80 k *	63.2 k	52.1 k	30 k *	27 k *

* Indicates specimen did not fail

8.0 ANALYSIS

8.1 Comparison to AASHTO Guide Specification

In 2008, AASHTO published the Guide Specifications for Bridges Vulnerable to Coastal Storms (referred to as the *Guide Specification*) to help designers quantify the wave loads experienced by coastal bridges. There are three cases considered in the guide:

1. Maximum quasi-static vertical force and associated forces and moment
2. Maximum quasi-static horizontal force and associated forces and moment
3. Assumed prorated overhang design forces

Case 3 is not considered in the present work. Since the vertical force is the controlling force for the failure of the superstructure, only Case 1 is considered. Case 2 is the controlling case in determining the lateral demands on the substructure.

Input values for the AASHTO *Guide Specification* calculation were based on the geometric properties of the laboratory test performed by Bradner (2008), and compared to the values calculated in the *Guide Specification* using a level I analysis. The test used from Bradner's experiment in this study created storm conditions similar to Hurricane Katrina. A summary of the values used is shown in

Table 7.

Table 7: Comparison of Input Parameters for AASHTO *Guide Specification*

<i>Parameter</i>	<i>Bradner Experimental Value</i>	<i>AASHTO Level I Analysis</i>
D (ft)	30	30
Zc (ft)	1.25	1.25
F (mi)	N/A	6 (Assumed)
Tp (sec)	6	5.2
Hs (ft)	8.2	10.0
Hmax (ft)	14.8	18.1
λ (ft)	125 (Assumed)	129.7

The *Guide Specification* prescribes the total wave-induced forces acting on the bridge superstructure, but does not specify distribution of these forces to individual anchorages. No test data are available in the literature to describe the distribution of forces to individual connections. Therefore, assuming a rigid superstructure, as observed in the field and hydrodynamic laboratory tests, a trapezoidal distribution of vertical loads results, as shown in Figure 43, is similar to the pile cap analogy used in geotechnical engineering and for live load distribution on exterior girders in the AASHTO-LRFD Specification. To develop more sophisticated and possibly non-uniform or nonlinear distributions would require detailed hydraulic tank models that have not been conducted previously or numerical hydrodynamic finite element analysis techniques, which are only now emerging and are not practical. Given the large uncertainties in the design parameters and assumptions, this linear distribution of forces is reasonable.

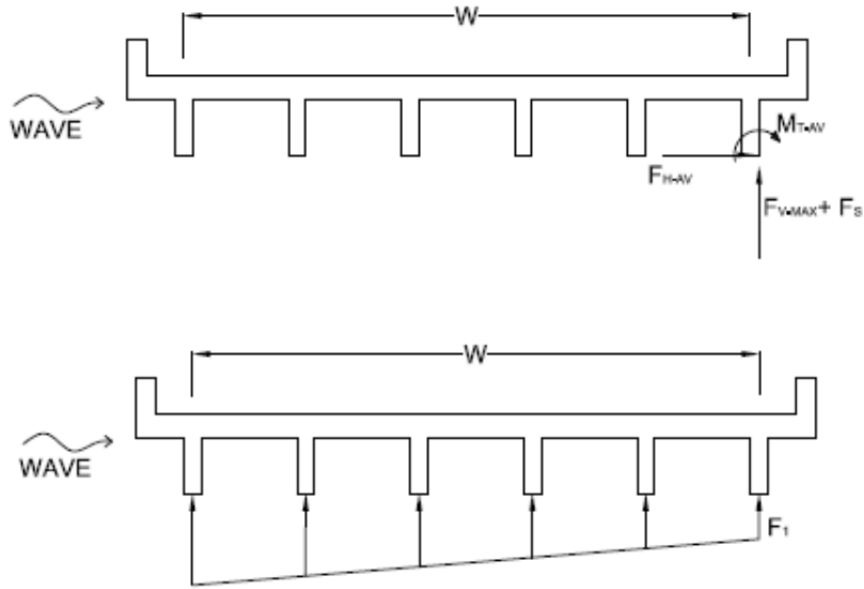


Figure 43: Assumed load distribution for typical bridge section assuming rigid superstructure.

The horizontal load is assumed to be shared equally among all anchorage points. Using the maximum vertical force and overturning moment calculated by the *Guide Specification* methodology and enforcing equilibrium conditions with an assumed linear distribution of forces to the regularly spaced girders, the magnitude of the vertical force acting at each girder line can be calculated by solving the following set of equations:

$$F_1 = \frac{F_V - s \cdot m \sum_{i=1}^{n-1} i}{n} \quad [1]$$

$$m = \frac{n \cdot M_{T-AV} - s \cdot F_V \sum_{i=1}^{n-1} i}{n \cdot s^2 \sum_{i=1}^{n-1} i^2 - s^2 \left(\sum_{i=1}^{n-1} i \right)^2} \quad [2]$$

The maximum vertical force acting on the off-shore anchorage can be determined as:

$$F_{MAX} = F_1 + m(n-1)s \quad [3]$$

where:

F_V = Total vertical force ($F_{V_MAX} + F_s$) (kN or kip)

F_1 = Vertical force distributed to on-shore girder (kN or kip)

F_{V_MAX} = Maximum vertical force per unit length of bridge (kN/m or kip/ft)

F_{Max} = Maximum vertical force acting on the off-shore girder (kN or kip)

M_{T-AV} = Associated trailing edge overturning moment per unit length of bridge (kN-m/m or kip-ft/ft)

m = slope of distribution (kN/m or kip/ft)

n = Number of girders

s = Girder spacing (m or ft)

F_1 = Distributed vertical force at on-shore girder (kN or kip)

m = slope of distribution (kN/m or kip/ft)

Figure 44 shows the wave load demands for a bridge span of the type considered in the present research. The vertical load is calculated from the *Guide Specification* and includes the bridge self-weight for a range of maximum wave heights. The maximum load calculated is based on 12 anchorage points per span (one on each end of the girders). Also noted on the figure are the failure loads of the different connection specimens - inclusive of the self-weight of the span, and the measured load maximum from Bradner's research (2008). A sample calculation is contained in Appendix F.

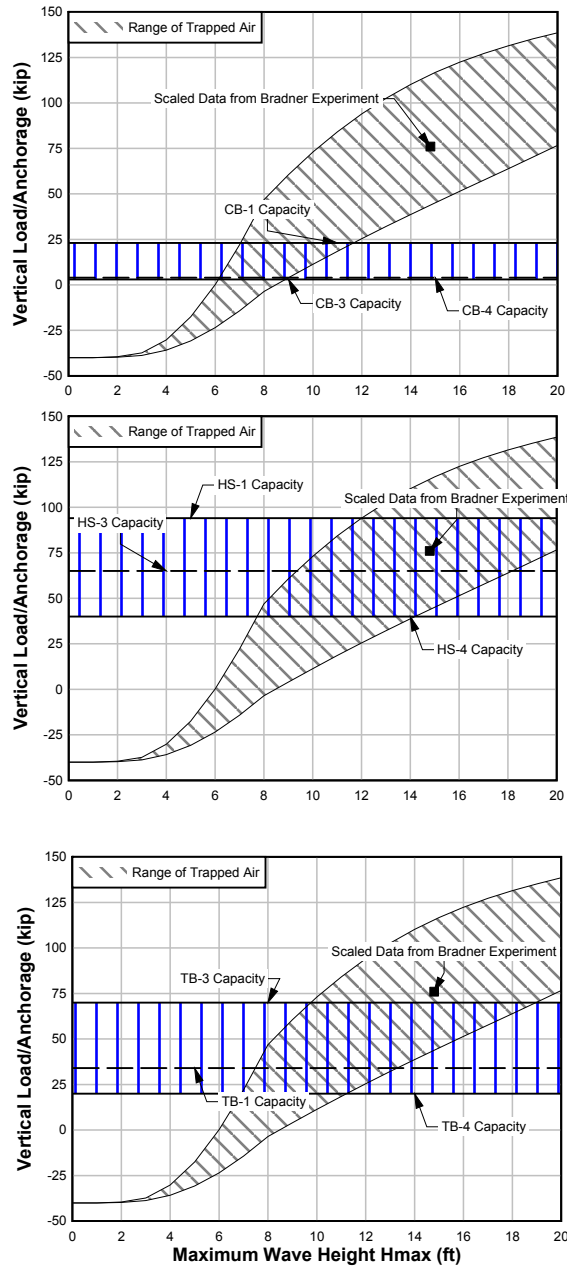


Figure 44: Maximum vertical load per anchorage - 12 anchor points used on the bridge.

Assuming the maximum amount of trapped air, none of the three anchorage designs were sufficiently strong to carry the loads prescribed by the *Guide Specification*. In service, bridges with the TB and CB anchorages connect every girder to the pile cap while the

Escambia Bay Bridge, with the HS detail, was only anchored at the exterior girders. While anchoring every girder would increase the overall bridge resistance, it would still not be sufficient to resist the forces prescribed by the *Guide Specification* if there is significant air trapped below the bridge deck. Even connection HS-1 was only able to sustain a maximum wave height of 11.8 feet when maximum entrapped air is considered (Figure 44).

Figure 45 shows horizontal load prescribed by the *Guide Specification* for bridges with 12 anchorages and four anchorages. As seen here, all anchorage types have sufficient strength to resist the horizontal forces if all girders are anchored (for Bradner's test conditions). The Escambia Bay Bridge only anchored the exterior girders of a span, and utilized the HS anchorage, which has sufficient strength to resist the prescribed horizontal loads from the *Guide Specification*. The horizontal force component of the wave loading is not as large as the net vertical force components, but when combined, the forces can act to sweep bridges from the substructure upon failure of the anchorages.

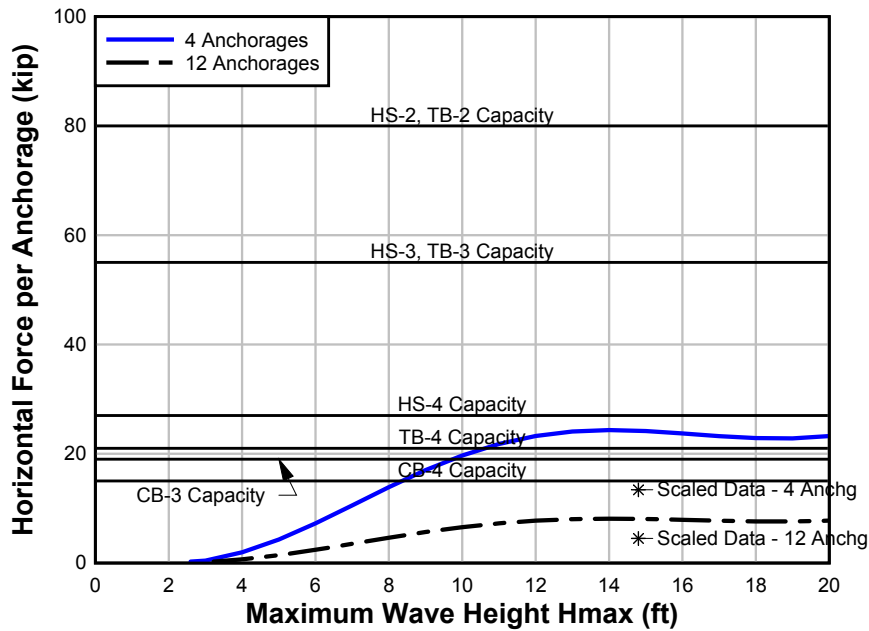


Figure 45: Associated horizontal force vs. maximum wave height for different numbers of anchor points and anchorage types.

The *Guide Specification* provides loads for the strength and extreme-event limit states. No commentary is made on the serviceability of bridges for hurricane wave loads. The HS anchorage did not exhibit strand slip, and only showed superficial cracking. The separation of the embedded steel plate from the concrete may expose the headed studs to corrosion, but should not affect the performance of the anchorage under service loads. Both the CB and the TB anchorages exhibited strand slip during testing, which can affect the performance of the girder under service loads. Cracking at relatively low load levels may accelerate corrosion of the prestressing strands, as chlorides can quickly reach the steel through the cracks. Corrosion of the strand will adversely impact the long-term durability of the girders. Figures comparing the load upon initiation of strand slip and initiation of cracking to the predicted *Guide Specification* loads can be found in Appendix F.

8.2 Comparison to ACI 318-08

The anchor capacity for each of the anchorage designs was calculated according to ACI 318-08 and compared to the experimental results. The ACI methods included embedded partial safety factors and resistance factors. Analyses were performed using measured concrete and steel material properties that are shown in Table 8. A sample calculation can be found in Appendix E.

Table 8: Material Properties for ACI Calculations

<i>Element</i>	<i>fc' (psi)</i>	<i>ft (ksi)</i>	<i>fv (ksi)</i>
Anchor Bolts – CB, TB	-	75	48
Anchor Bolts - HS	-	37.5	24
Through Bolts	-	-	75.3
Headed Studs	-	78.5	38.3
Concrete – CB	5200	-	-
Concrete – HS	5200	-	-
Concrete - TB	5600	-	-

For the CB anchorage, Table 9 shows the failure modes considered and the predicted failure load associated with each mode. Failure modes associated with the steel angles were not considered. The dead load of the bridge superstructure is not included in the predicted failure load in Table 9. Using the minimum capacity, the predicted failure mode of the anchorage was shear breakout of the girder concrete. This value was 9% higher than the experimental value of 23 kips.

Table 9: CB Failure Modes

<i>Failure Mode</i>	<i>Load (Kips)</i>
Tension Failure Anchor Bolts	331
Tensile Concrete Breakout – Pile Cap	31
Shear Failure Anchor Bolts	353
Shear Concrete Breakout – Pile Cap	46
Shear Concrete Breakout – Girder	25
Concrete Pryout – Anchor Bolts	62

Table 10 shows the failure modes considered for the HS connections. The controlling failure mode was concrete pullout of the group of headed studs, followed by the tension concrete breakout of the pile cap. This is not consistent with the failure modes observed in the field after Hurricane Ivan. The failures observed on the I-10 Escambia Bay Bridge were failures of the anchor bolts, as well as failure of the headed studs where they connected with the embedded steel plate. The observed failure during this study was tension failure of the headed studs at 94 kips. The value in Table 10 includes a partial safety factor of 0.9. Removing that factor, the failure load is predicted at 95.5 kips, or 1.5% higher than the experimental value.

Table 10: HS Failure Modes

<i>Failure Mode</i>	<i>Load (Kips)</i>
Tension Failure Anchor Bolts	53

Tension Failure Headed Studs	86
Tension Concrete Breakout – Pile Cap	15
Tension Concrete Breakout – Girder	196
Tension Pullout Headed Studs	29/Stud
Shear Failure Anchor Bolts	57
Shear Failure Headed Studs	47
Shear Concrete Breakout – Pile Cap	26
Shear Concrete Breakout – Girder	149
Concrete Pryout – Anchor Bolts	29
Concrete Pryout – Headed Studs	12

Table 11 shows the failure modes considered for the TB connections. The controlling failure mode was shear concrete breakout in the girder; however, the predicted strength was less than the measured failure load. This is because the through bolts are not rigid and are able to deform under load within the concrete, thus applying more force on the outer edges of the flange (near the surface), resulting in a progressive failure.

Table 11: TB Failure Modes

<i>Failure Mode</i>	<i>Load (Kips)</i>
Tension Failure Anchor Bolts	331
Tension Concrete Breakout – Pile Cap	21
Shear Failure Anchor Bolts	353
Shear Failure Through Bolts	226

Shear Concrete Breakout – Girder	8
Concrete Pryout Anchor Bolts	46

Based on these results, the capacity of the connections can be reasonably predicted using current design methods in ACI 318. The failures of the connections observed in recent hurricanes should not be surprising considering the forces produced by hurricane-induced wave loads.

Future designs should design the connections to resist the prescribed AASHTO Guide forces using ACI 318 approaches, and include the strength of connecting plates, angles and anchor bolts. Based on the observed responses of the connections tested, future connection designs should be attached to the girders higher up the stem, and include connection of the end diaphragms which would likely produce higher strength and less ancillary cracking or other concrete damage.

9.0 CONCLUSIONS

Recent strong hurricanes have caused significant damage to the transportation infrastructure along the U.S. Gulf Coast. Prestressed concrete bridge damage was most often attributed to failure of the superstructure-to-substructure connections. Based on a survey of DOT's along the Gulf Coast, three anchorages types were identified as commonly used. These connections were the headed stud (HS), clip bolt (CB), and through bolt (TB). These connections were used in the present experimental study. Each of the three anchorages types was subjected to four different loading conditions: vertical pseudo-static cyclic loading; horizontal pseudo-static cyclic loading; simultaneous horizontal and vertical pseudo-static cyclic loading; and dynamic loading (with simultaneous vertical and horizontal forcing) based on the recorded time-history forces recorded from a hydrodynamic model of a 1/5-scale bridge as reported by Bradner (2008).

Based on the reported experimental results and analysis, the following conclusions are presented:

- The headed stud (HS) anchorage exhibited the most robust performance of the three anchorages considered. It had higher load capacity and exhibited minimal ancillary damage to the prestressed concrete girders even at failure.
- Failure of the HS anchorage was controlled by the performance of the steel studs, which is predictable and allows the anchorage to be detailed to limit forces transferred to the substructure. Details such as these, with well-defined strength characteristics, and those that produce little collateral damage to the concrete are preferable.

- The clip bolt (CB) anchorage did not provide sufficient strength to resist wave loads produced by a storm with the intensity of Hurricane Katrina for the bridge configuration considered. It was the weakest of the connections considered.
- The through bolt (TB) anchorage resisted higher loads than the CB anchorage, and exhibited significant damage throughout the section of the prestressed girder at the level of the prestressing strands.
- The CB and TB anchorages exhibited concrete cracking and strand slip prior to failure, which may impact long-term performance of the bridge after survival of the hurricane event.
- None of the anchorage types exhibited sufficient strength to resist the vertical loads prescribed by the AASHTO *Guide Specification* for the bridge configuration considered when wave heights exceeded 11.8 feet (3.6 meters) and significant trapped air is present. The HS anchorage would be sufficient to resist the prescribed vertical force if all girders are attached, and there is entrapped air representative of those measured on the reduced-scale hydrodynamic model by Bradner (2008).
- Existing bridges deploying the connection types tested here may require retrofitting to ensure that they are not damaged or destroyed in future large hurricanes.
- Connections between the substructure and superstructure that rely on the concrete flanges to resist wave-induced uplift forces, like the CB and TB details investigated, are not ideal choices for retrofitting existing bridges. Retrofit designs may perform better if anchored higher into the stems and end diaphragms, and additional research focused on retrofitting would help inform such designs.

10.0 BIBLIOGRAPHY

- Alabama DOT. (2009). Miscellaneous Superstructure Details. E-mail message to author by Robbie Chambless, April 21, 2009.
- American Association of State Highway and Transportation Officials. (2008). "Guide Specification for Bridges Vulnerable to Coastal Storms." 1st edition.
- American Concrete Institute. (2008). "Building Code Requirements for Structural Concrete (ACI318-08).
- Bode, H., & Roik, K. (1987). Headed Studs - Embedded in Concrete and Loaded in Tension. *ACI Special Publication*, 103, 61-88.
- Bode, H., Leffer, A., & Mensinger, M. (2000). The Influence of the Stress Range History on the Fatigue Behavior of Headed Studs. *Composite Construction in Steel and Concrete IV* (p. 5). Banff, Alberta, Canada: ASCE.
- Bradner, Christopher (2008). Large-Scale Laboratory Observations of Wave Forces on a Highway Bridge Superstructure. Master's Thesis. Oregon State University.
- Chen, Q., Wang, L., & Zhao, H. (2009). Hydrodynamic Investigation of Coastal Bridge Collapse during Hurricane Katrina. *Journal of Hydraulic Engineering*, 135 (3), 175-186.
- Douglass, S., Chen, Q., & Olsen, J. (2006). Wave Forces on Bridge Decks Draft Report. Coastal Transportation Engineering Research and Education Center. University of South Alabama
- Douglass, S., Hughes, S., Rogers, S., and Chen, Q. (2004). Impact of Hurricane Ivan on the Coastal Roads of Florida and Alabama: A Preliminary Report. Coastal Transportation Engineering Research and Education Center. University of South Alabama.
- Eligehausen, R., & Balogh, T. (1995). Behavior of Fasteners Loaded in Tension in Cracked Reinforced Concrete. *ACI Structural Journal*, 365-379.
- Hanswille, G., Porsch, M., & Ustundang, C. (2007). Resistance of Headed Studs Subjected to Fatigue Loading, Part I: Experimental Study. *Journal of Constructional Research*, (63) 4, 475-484.

- Huang, W., & Xiao, H. (2009). Numerical Modeling of Wave Force Acting on Escambia Bay Bridge Deck During Hurricane Ivan. *Journal of Waterway, Port, Coastal, and Ocean Engineering*, (135)4, 164-175.
- Feldmann, M., Gesella, H., & Leffer, A. (2006). The Cyclic Force-Slip Behaviour of Headed Studs under Non Static Service Loads: Experimental Studies and Analytical Descriptions. *ASCE Conf. Proceedings* (p. 53). Kruger National Park, Berg-en-Dal, Mpumalanga, South Africa: ASCE.
- Florida DOT. (2008). Design Build Contracts Status as of: 09/30/2008. Retrieved from Florida Department of Transportation:
<http://www.dot.state.fl.us/construction/DesignBuild/DBGGeneral/DesignBuildReport.pdf>
- Kannel, J., French, C., and Stolarski, H. (1997). Release Methodology of Strands to Reduce End Cracking in Pretensioned Concrete Girders. *PCI Journal*, (42)1, 42-54.
- Klingner, R., and Mendonca, J. (1992). Tensile Capacity of Short Anchor Bolts and Welded Studs: A Literature Review. *ACI Journal*, 270-279.
- Lam, D., & El-Lobody, E. (2005). Behavior of Headed Stud Shear Connectors in Composite Beam. *Journal of Structural Engineering*, 131 (1), 96-107.
- Louisiana DOT. (2009). Miscellaneous Span and Girder Details. E-mail message to author by Arthur D'Andrea, May 18, 2009.
- Marin, J., & Sheppard, M. (2009). Storm Surge and Wave Loading on Bridge Superstructures. *ASCE Conf. Proceedings* (p. 557). Austin, TX.
- Nickas, William. E-mail message to author, April 08, 2009.
- Oh, B., & Kim, E. (2000). Realistic Evaluation of Transfer Lengths in Pretensioned Prestressed Concrete Members. *ACI Structural Journal*, 97 (6), 821-830.
- Okeil, A., & Cai, C. (2008). Survey of Short and Medium Bridge Span Damage Induced by Hurricane Katrina. *Journal of Bridge Engineering*, 13(4), 377-387.

- Padgett, J., DesRoches, R., Nielson, B., Yashinsky, M., Kwon, O., Burdette, N., et al. (2008, January/February). Bridge Damage and Repair Costs from Hurricane Katrina. *J. of Bridge Engineering* , 6-14.
- Robertson, I., Riggs, H., Yim, S., and Young, Y. (2007). Lessons from Hurricane Katrina Storm Surge on Bridges and Buildings. *Journal of Waterway, Port, Coastal, and Ocean Engineering*, 133 (6), 463-483.
- Schumacher, T., Higgins, C., Bradner, C., & Cox, D. (July 2008). Large-Scale Wave Flume Experiments on Highway Bridge Superstructures Exposed to Hurricane Wave Forces. *The Sixth National Seismic Conference on Bridges and Highways*. Charleston, South Carolina.
- Veljkovic, M., & Johansson, B. (2006). Residual Static Resistance of Welded Stud Shear Connectors. *Composite Construction in Steel and Concrete V* (p. 49). Kruger National Park, Berg-en-Dal, Mpumalanga, South Africa: ASCE.
- Yong, Y.-K., Gadegebeku, C. B., & Nawy, E. G. (1987). Anchorage Zone Stresses of Beams Subjected to Shear Forces. *Journal of Structural Engineering* , 1789-1805.

APPENDICES

Appendix A: Self-Weight of Bridge Span

A calculation of the self-weight of a typical bridge superstructure span is presented below.

Element	quantity	area in ²	length ft	volume ft ³	unit weight pcf	total weight kip
Deck	1	2688	56.8	1060.9	150	159.1
Girder	6	559.5	56.8	220.8	150	198.7
Diaphragm	3	272	27.1	51.2	150	23.0
Curb	2	252	56.8	99.5	150	29.8
Railing	2	143	56.8	56.4	150	16.9
Railing spt.	20	132	2.25	2.1	150	6.2
Wearing	1	1080	56.8	426.3	140	59.7
Total						493.5

Appendix B: Instrumentation

The instrumentation plans for the 12 specimens are presented below:

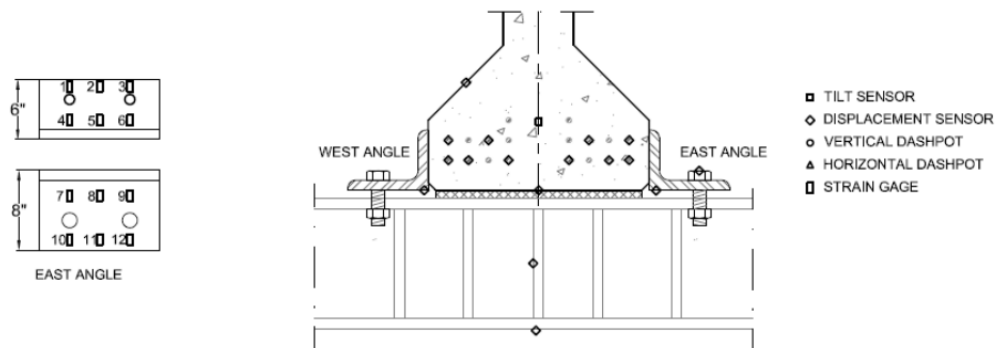


Figure B- 1: CB-1 Instrumentation Plan

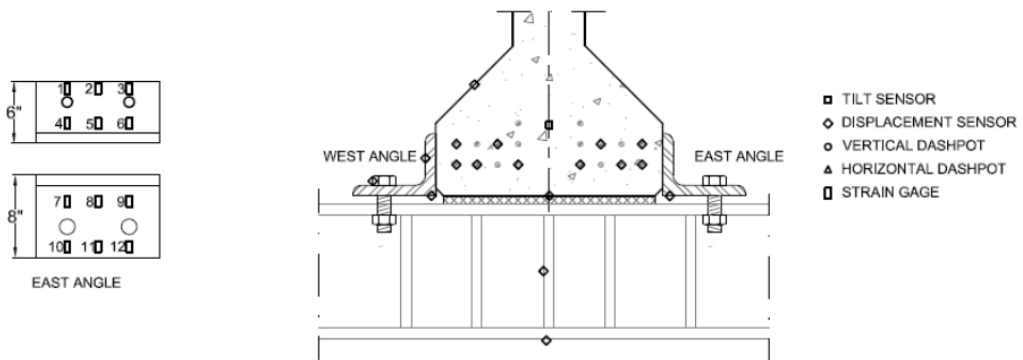


Figure B- 2: CB-2 Instrumentation Plan

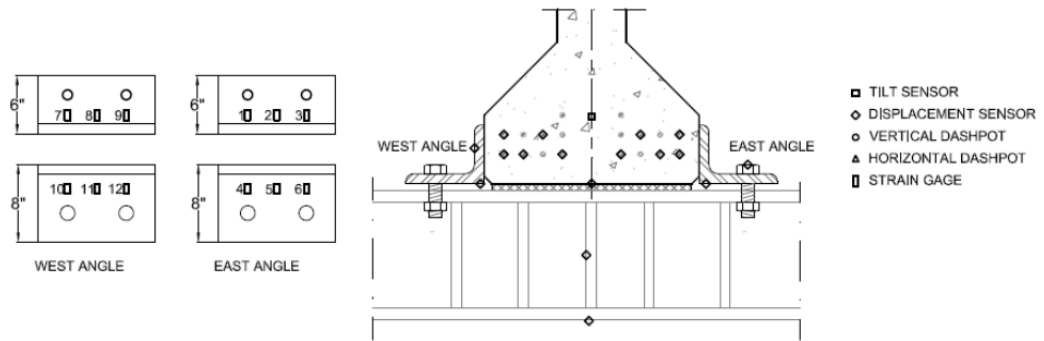


Figure B- 3: CB-3 Instrumentation Plan

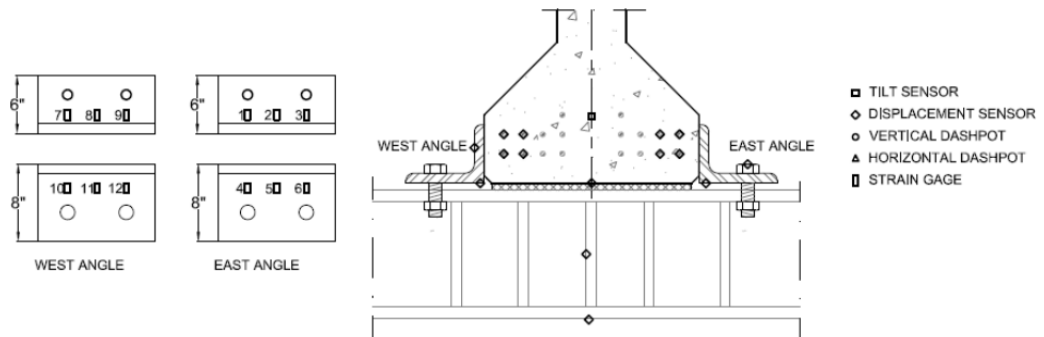


Figure B- 4: CB-4 Instrumentation Plan

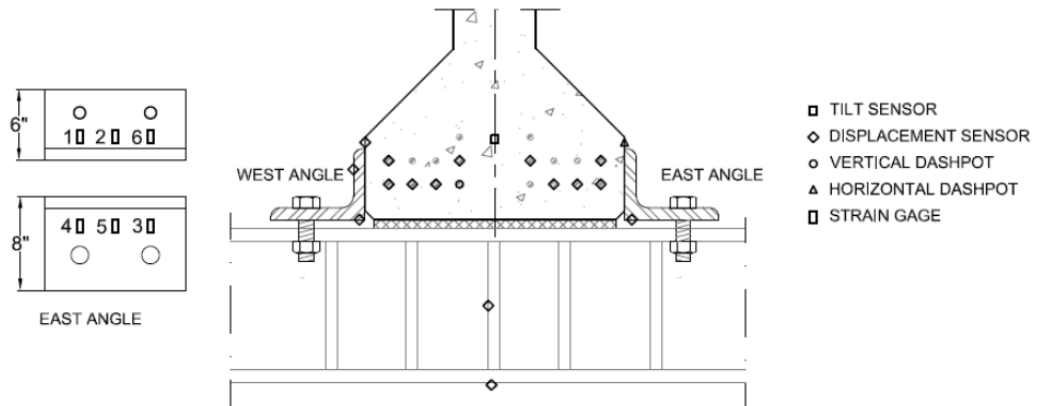


Figure B- 5: TB-1 Instrumentation Plan

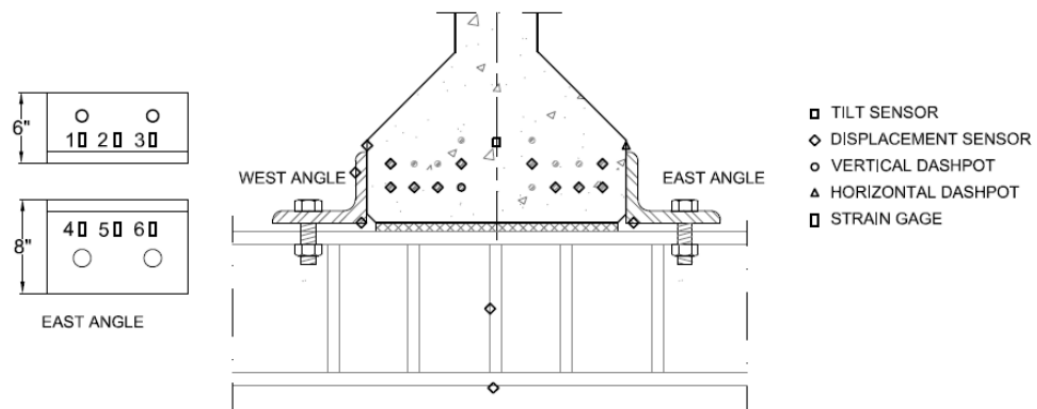


Figure B- 6: TB-2 and TB-3 Instrumentation Plan

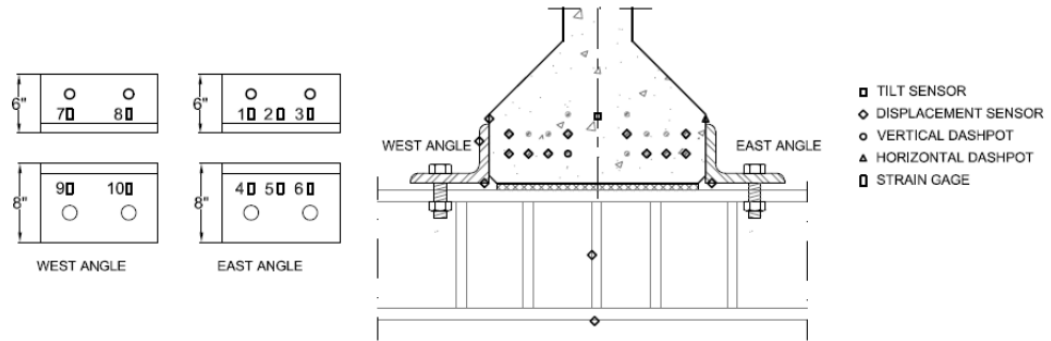


Figure B- 7: TB-4 Instrumentation Plan

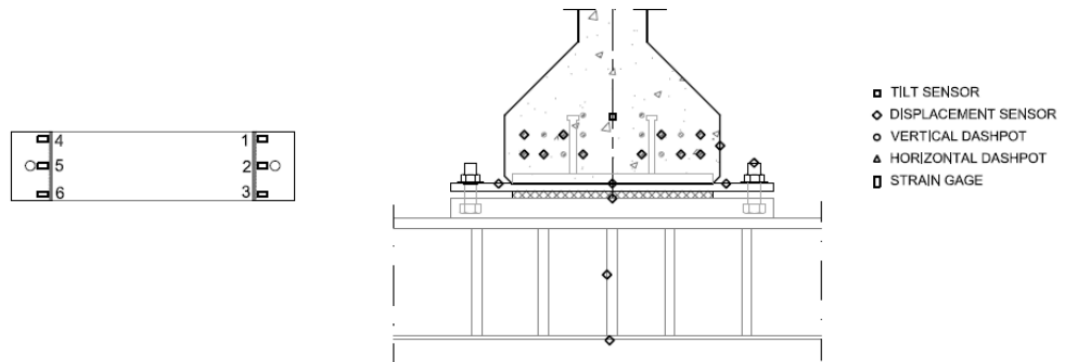


Figure B- 8: HS-1 Instrumentation Plan

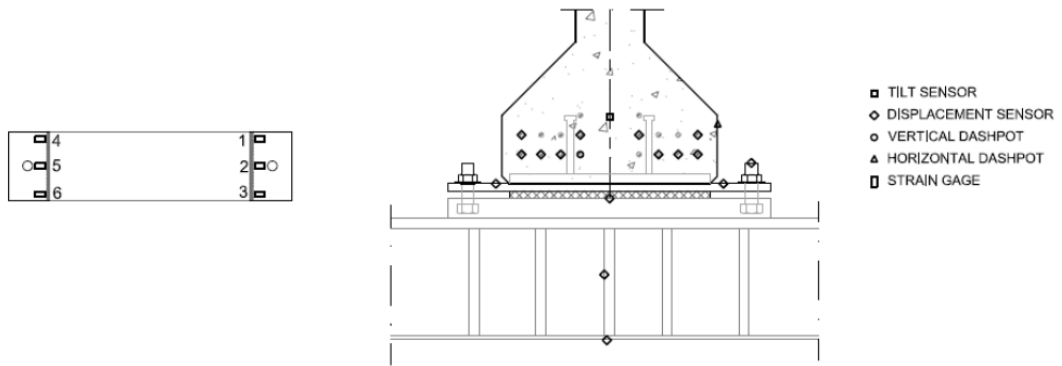


Figure B- 9: HS-2, HS-3, and HS-4 Instrumentation Plan

Appendix C: Anchorage Details

Selected departments of transportation were surveyed to determine common anchorage details along the Gulf Coast to include in this study. Three anchorage types were chosen. The original drawings are shown here.

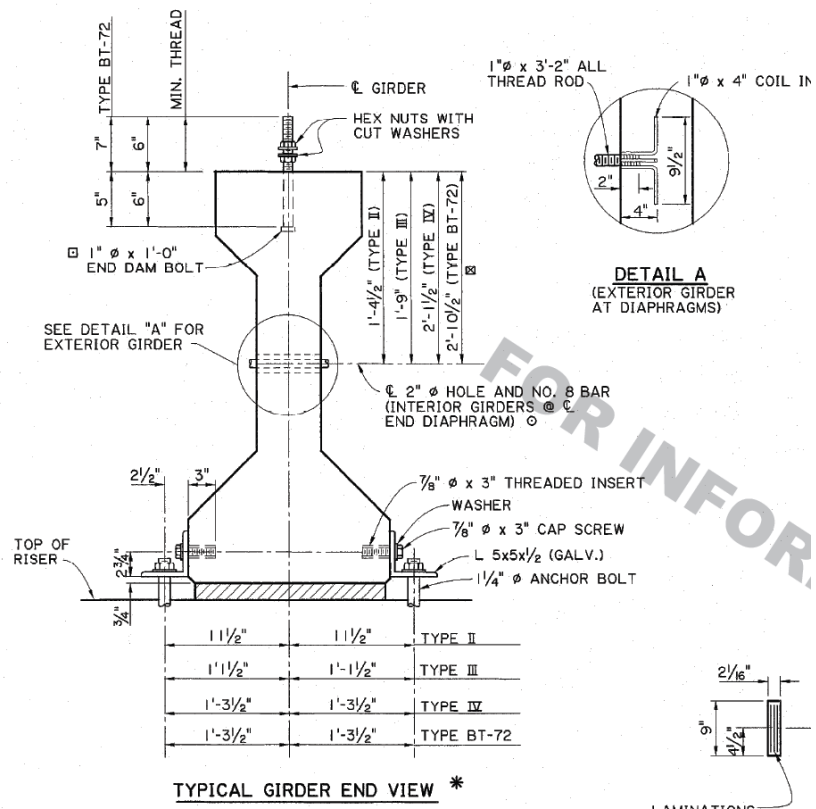


Figure C- 1: LADOT Misc. Span and Girder Details

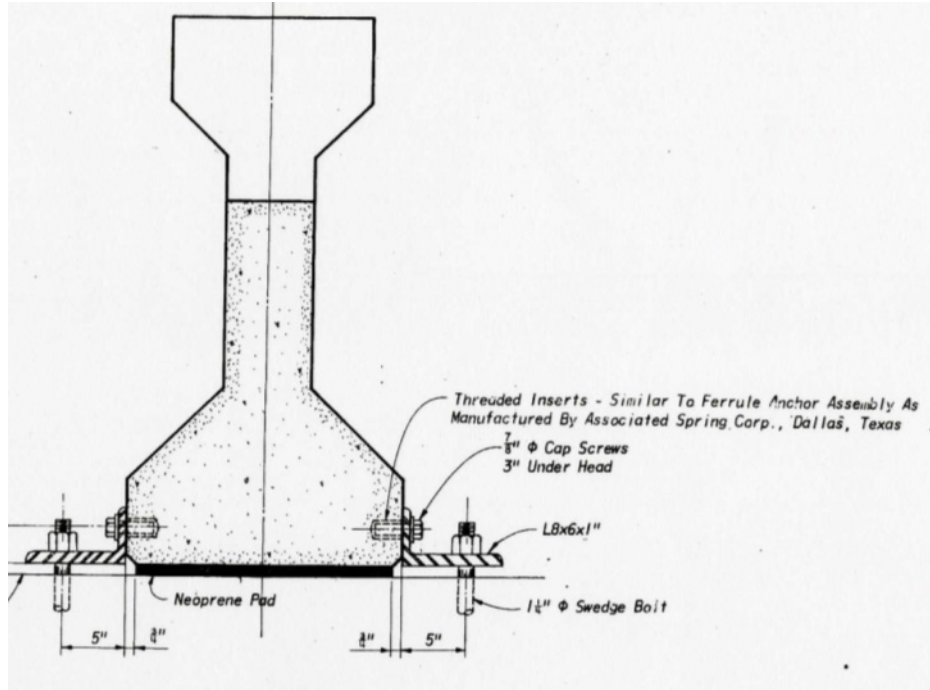


Figure C- 2: ALDOT Girder Details – Mobile Bay Crossing

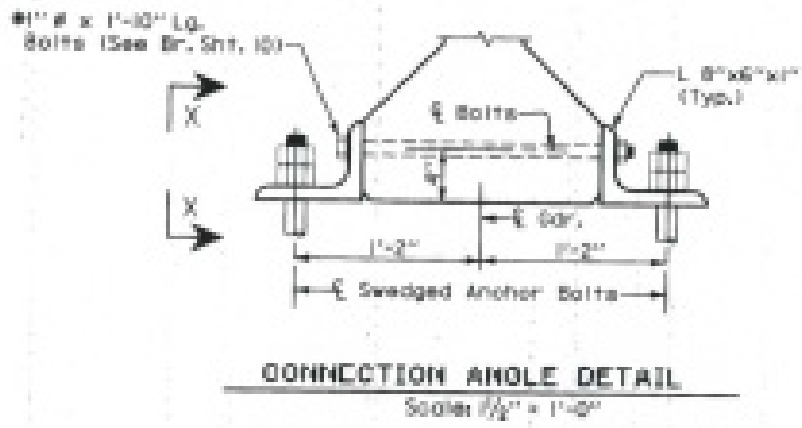


Figure C- 3: ALDOT Typical Details

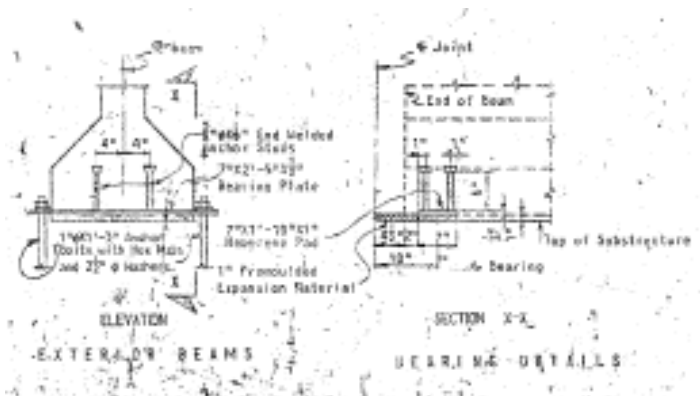


Figure C- 4: I-10 Escambia Bay Anchorage Details (FDOT)

The threaded inserts used for this study are the F-5 threaded inserts produced by Dayton Superior. The 7/8-inch diameter inserts are used per the plans provided by the Alabama and Louisiana DOTs.

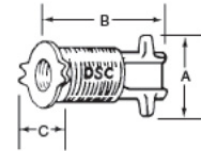
NC Threaded Inserts
 For Suspending, Connecting
 and Anchoring to Concrete



F-5 Threaded Insert

The Dayton Superior F-5 Threaded Inserts have National Course (NC) threads and are recommended for use under permanent loading conditions. This insert has been approved by the Board of Standards and Appeals for use in New York City under Calendar No. 447-60SM.

The F-5 insert is cast from ductile iron that meets ASTM A-395, Grade 60-40-18.



**F-5
 Threaded Insert**

To Order:
 Specify: (1) quantity, (2) name,
 (3) bolt diameter.
Example:
 200, F-5 Threaded Inserts, 3/4" bolt diameter.

F-5 Threaded Insert Selection Chart					
Bolt Diameter and Threads per Inch	Tension Safe Working Load	Bolt Engagement	A	B	C
1/2" – 13	1,500 lbs.	15/16"	1-5/8"	2-1/2"	1-5/8"
5/8" – 11	2,000 lbs.	3/4"	1-5/8"	3"	1-5/8"
3/4" – 10	2,500 lbs.	7/8"	1-13/16"	3"	1-7/8"
7/8" – 9	3,000 lbs.	1-5/16"	2-1/2"	3-3/8"	2-5/8"
1" – 8	3,000 lbs.	1-5/16"	2-1/2"	3-3/8"	2-5/8"

Safe Working Load provides a factor of safety of approximately 3 to 1 when the insert is properly embedded in 3,000 psi normal weight concrete.

Figure C- 5: F-5 Insert Technical Data

Appendix D: Material Properties

The AASHTO III sections were fabricated by Knife River Corporation in Harrisburg, OR.

The mix design and properties are shown below.


 KNIFE RIVER CORP.		Control #	183575	183576				
		Batch Size	5.00	CY			Test Meter	922
		Batch Weights (lbs.)			Add Water Quantities (gals.)			
PROJECT TITLE	OSU Test Beams	Cement I					Water at Plant	113 (WP)
PROJECT NO.	98061	Cement III	2332	(CW)			Water at Jobsite	(WA)
PRODUCT TYPE	AASHTO TYPE III	Flyash		(FA)			Total Water	113 (TG)
BED NO.	4	S. Fume		(SF)			Weight of Water	942 (WW)
MARK NO.		CA #1 1/2	3750	(CA1)				
INSPECTION		CA #2 3/4	5360	(CA2)				
DATE	Fri. 08/14/09	Sand	7560	(SND)			Admixtures (ozs.)	
CONCRETE MIX NO.	C47N3	Water	942	(WW)			Air Entrainment	(AEA)
CEMENT TYPE	Ashgrove Type III	Admixture	4.50	(AW)			Polyheed	72 (PH)
CEMENT CONTENT	470. lbs cement / CY	TOTAL	19949	(TW)			100XR	(XR)
							Glenium	(GL)
							Pozzolith	(POZ)
							Delvo	(DEL)
							Total Admixtures	72 (TA)
							Admixture Weight	4.50 (AW)
TESTS		VALUES		Unit Weight, Yield, and Cement Content				
SLUMP/SPREAD/VSI	3.75	Concrete + Pot:		43.90				
CON. TEMP.	76.00	Pot Weight (tare):		7.30			Cement Content	466.70 lbs./cy.
AMB. TEMP.	72.00	Calibration:		4.040			S.K.	4.96
POT WT.	43.90	UNIT WEIGHT:		147.86 lbs./cu. ft.				
AIR	2.0						Yield	5.00
RELEASE STRENGTH		ACTUAL		Available Water				
DESIGN :	3500	3790		Batch Weight	Absorption		Free Moisture	Total Water (%)
28 DAY:	5000	3930		CA1	3750	2.40	0.4	14.94
		3860		CA2	5360	2.40	0	0.00
				Sand	7560	2.99	2.3	169.97
HEAT START	20:00			Available Water (lbs.)				
				CA1	14.940		Water Added:	942.42 (WW)
				CA2	0.000		Admixtures:	4.50 (TA)
RELATIVE YIELD	1.00			Sand	169.971		Total Available Water:	1131.83 (TAW)
W/C RATIO	0.49			Total	184.911			

Figure D- 1: Knife River Concrete Mix Data

For each of the six test beams, test-day cylinders were broken to determine the concrete strength at testing. The test results are presented here.

Table D- 1: Concrete cylinder compressive and tensile strengths

<i>Specimen</i>	f'_c (psi)	f_t (psi)
CB-1, CB-2	5216	471
CB-3, CB-4	5231	631
HS-1, HS-2	5190	543
HS-3, HS-4	5369	598
TB-1, TB-2	5545	594
TB-3, TB-4	5740	586
Average	5382	571

Steel tension coupon tests were performed to verify the strength of the headed studs and mild steel reinforcing. The stress/strain diagrams are presented here.

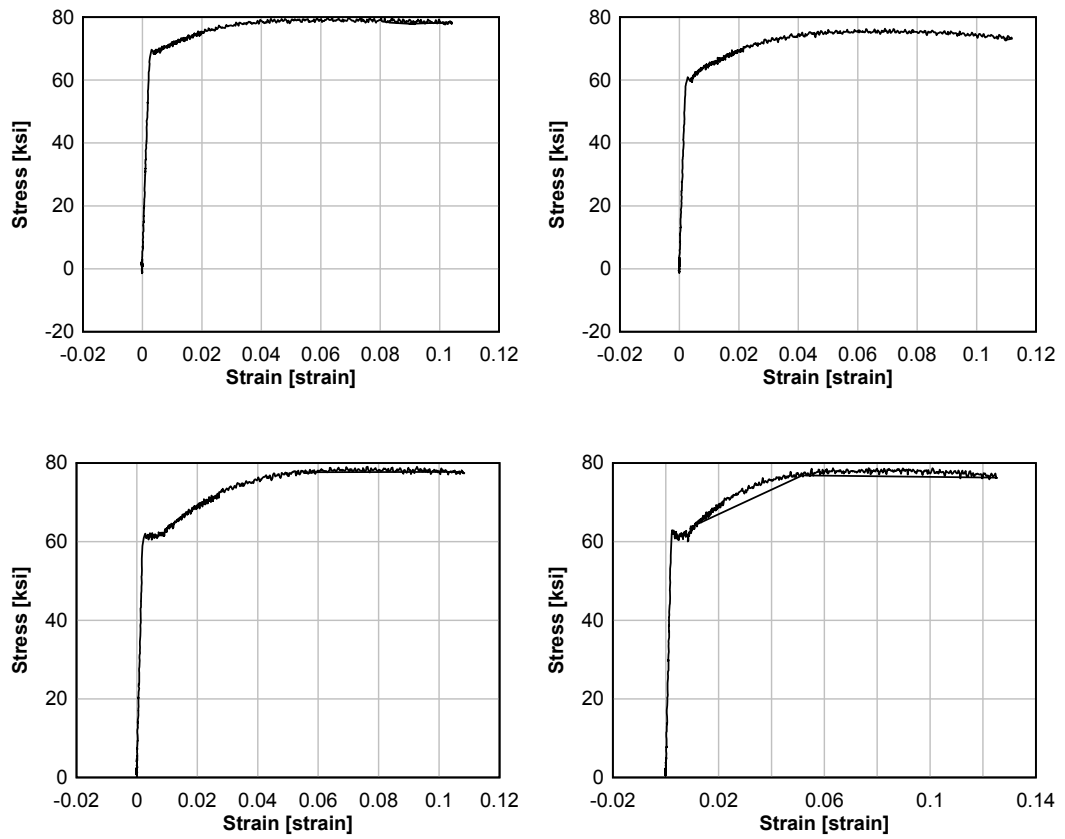


Figure D- 2: Headed Stud Stress/Strain Diagrams

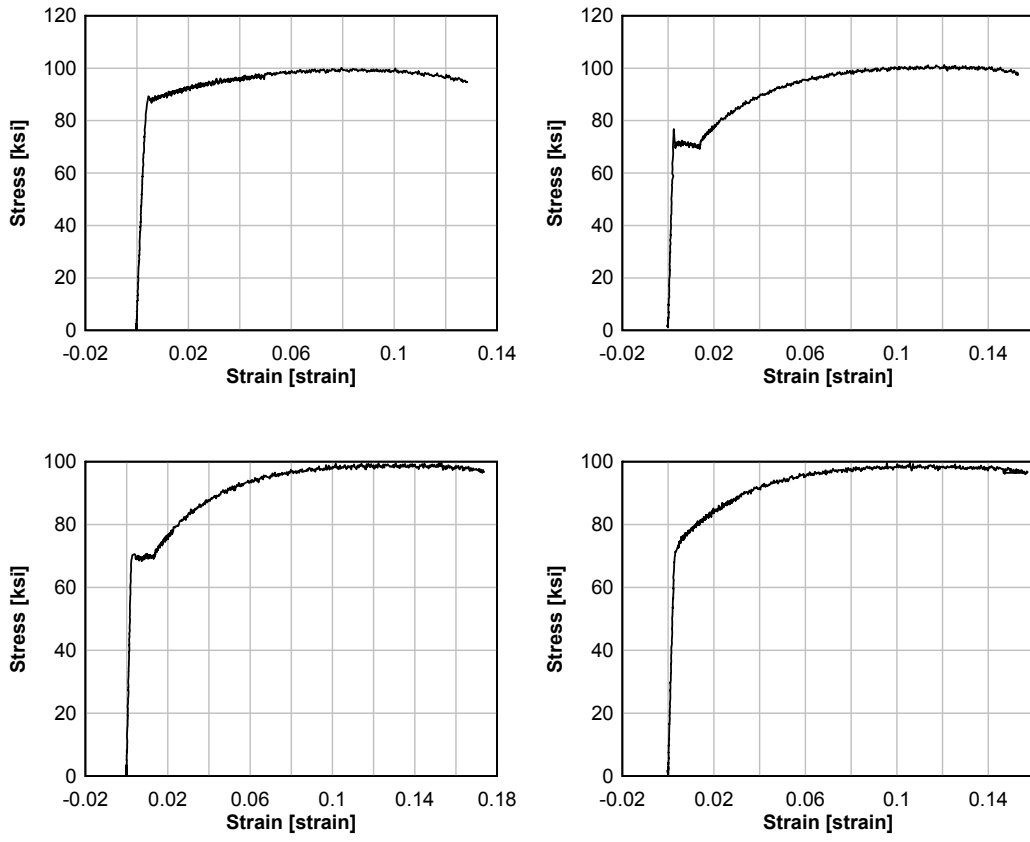


Figure D- 3: Mild Reinforcing Stress/Strain Diagrams

Appendix E: ACI 318 Calculations

ACI 318-08 was used to calculate the capacity of the concrete anchors for both the girder and pile cap. A sample calculation of a tension breakout and a shear breakout are shown here.

Tension Breakout: ACI 318-08 Section D.5.2

$$N_{cb} = \frac{A_{NC}}{A_{NCO}} (\Psi_{ec,N}) (\Psi_{ed,N}) (\Psi_{c,N}) (N_b) \quad (\text{EQ D-5})$$

Where:

$$A_{NCO} = 9h_{ef}^2$$

$$N_b = k_c \lambda \sqrt{f'_c} h_{ef}^{1.5}$$

And:

Ψ_1 = adjustment factor

A_{nc} = projected failure area for anchor group

A_{nc0} = projected failure area for one anchor with large edge distances

N_b = concrete breakout strength

h_{ef} = anchor embedment

k_c = 17 for post installed anchors

λ = 1.0 for normal weight concrete

Shear Breakout: ACI 318-08 Section D.6.2

$$V_{cb} = \frac{A_{VC}}{A_{VCO}} (\psi_{ec,V}) (\psi_{ed,V}) (\psi_{c,V}) (\psi_{h,V}) (V_b) \quad (\text{EQ D-22})$$

Where:

$$A_{VCO} = 4.5 \cdot ca_1^2$$

$$V_b = \left[7 \left(\frac{l_e}{d_a} \right)^{0.2} \sqrt{d_a} \right] \lambda \sqrt{f'_c} Ca_1^{1.5}$$

And:

Ψ_i = adjustment factor

V_{nc} = projected failure area for anchor group

V_{nc0} = projected failure area for one anchor with large edge distances

V_b = concrete shear breakout strength

h_{ef} = anchor embedment

$l_e = h_{ef}$

$\lambda = 1.0$ for normal weight concrete

Ca_1 = smallest edge distance from anchor

d_a = Anchor diameter

Appendix F: AASHTO Calculations

The AASHTO Guide Specification for Bridges Vulnerable to Coastal Storms was used to calculate expected wave forces from Hurricane Katrina wave conditions at Escambia Bay, FL. A level-I analysis was performed to determine the input values for the calculation.

The 100-year design wind speed for Escambia Bay is 140 mph or 205.3 ft/sec. This is converted to a 10-minute design speed of 153.8 ft/sec. The 10-minute design speed is used to calculate the wind stress factor U_t^* , used in determining other input values.

$$U_t^* = 0.539U_{10\text{min}}^{1.23}$$

The wave period is determined by the following equation:

$$T_p = 7.54 \tanh \left[0.833 \left(\frac{gd}{U_t^{*2}} \right)^{3/8} \right] \tanh \left[\frac{.0379 \left(\frac{gF}{U_t^{*2}} \right)^{1/3}}{\tanh \left[.833 \left(\frac{gd}{U_t^{*2}} \right)^{3/8} \right]} \right] \frac{U_t^*}{g}$$

Where:

$$g = 32.2 \text{ ft/s}^2$$

F = Fetch length (assumed 6 miles)

d = Average depth over fetch length including surge = 20 ft

$$T_p = 5.04 \text{ sec}$$

The significant wave height and wavelength are calculated as follows:

$$H_s = 0.283 \tanh \left[0.53 \left(\frac{gd}{U_t^{*2}} \right)^{3/4} \right] \tanh \left[\frac{0.00565 \left(\frac{gF}{U_t^{*2}} \right)^{1/2}}{\tanh \left[0.53 \left(\frac{gd}{U_t^{*2}} \right)^{3/4} \right]} \right]$$

$$\lambda = \frac{gT_p^2}{2\pi} \left[\tanh \left(\frac{4\pi^2 d_s}{T_p^2 g} \right) \right]^{1/2}$$

Where:

$d_s = 20$ ft = water level at bridge including storm surge

$H_s = 8.5$ ft = significant wave height

$\lambda = 112.5$ ft = wavelength

The maximum wave height is considered to be 180% of the significant wave height, and the maximum distance from the storm water level to the design wave crest is considered to be 70% of the maximum wave height.

$H_{\max} = 13$ ft

$\eta_{\max} = 9.1$ ft

These values are used in the design case I to determine the wave loads. The procedure can be found in the guide specification. Assuming the vertical distance from the bottom of the superstructure cross section to the storm water level (z_c) is 0 ft, the results from design case I are as follows:

$$F_{vMAX} = 13.7 \text{ k/ft}$$

$$F_s = 4.5 \text{ k/ft}$$

$$F_{H_AV} = 1.3 \text{ k/ft}$$

$$M_{T_AV} = 375.2 \text{ k-ft/ft}$$

These forces are distributed to the anchorages using the pile cap analogy and equilibrium, as previously discussed.

Figure F- 1 shows the maximum vertical load per anchorage including the bridge self-weight, assuming only the exterior girders are anchored versus the maximum wave height. Figures showing the maximum vertical load assuming all girders are anchored can be found in the body text.

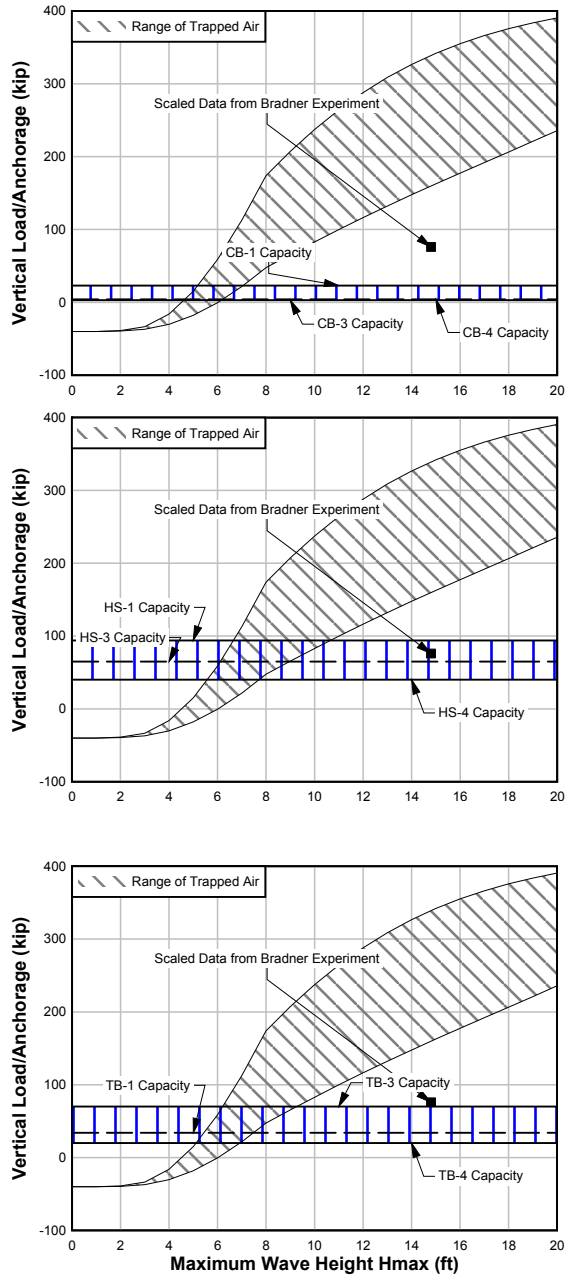


Figure F- 1: Maximum Vertical Load per Anchorage for Four Anchorage Points

Serviceability of bridges is not discussed in the AASHTO *Guide Specification*. Cracking and strand slip was detected in the CB and TB anchorages, making them susceptible to performance issues under service loads, as well as reduced long-term durability due to corrosion. Figures F-2, F-3 and F-4 show the range of strand slip initiation for the CB and TB anchorages compared to the predicted vertical loads per anchorage; including the superstructure self-weight and assuming all girders are anchored. Figure F- 5 and Figure F- 6 show the ranges of crack initiation for all girder types, including the superstructure self-weight and assuming all girders are anchored.

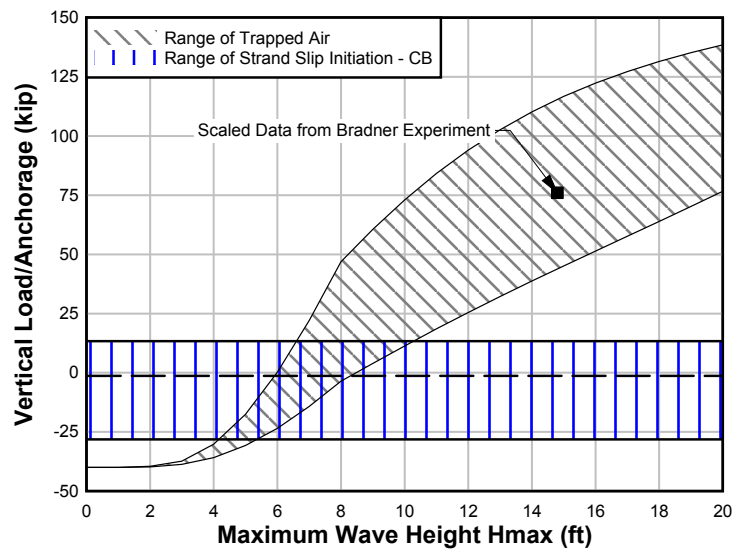


Figure F- 2: AASHTO Vertical Load per Anchorage and Strand Slip - CB Anchorage

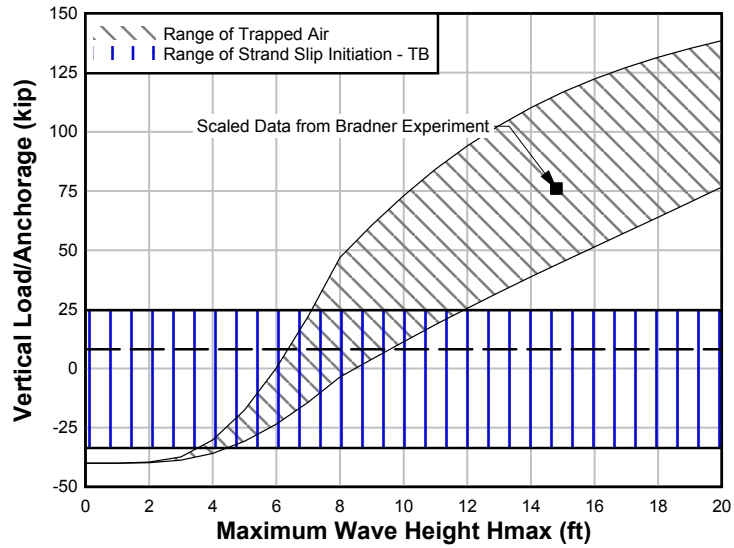


Figure F- 3: AASHTO Vertical Load per Anchorage and Strand Slip – TB Anchorage

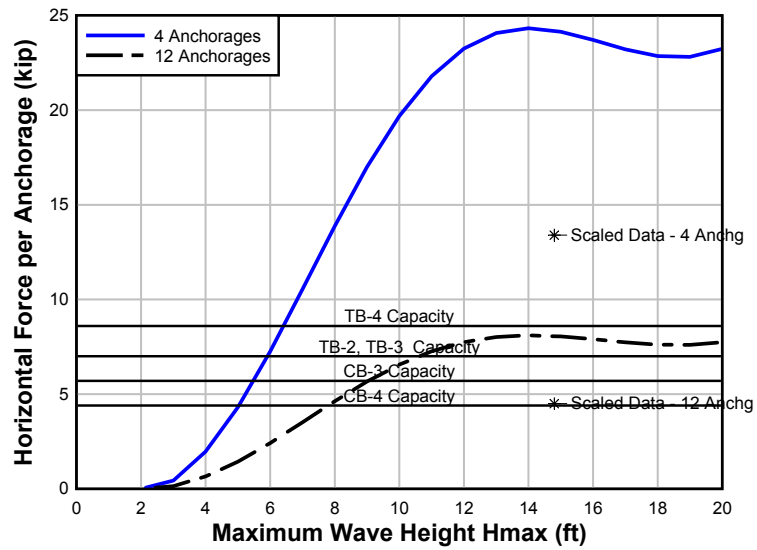


Figure F- 4: AASHTO Horizontal Load per Anchorage and Strand Slip

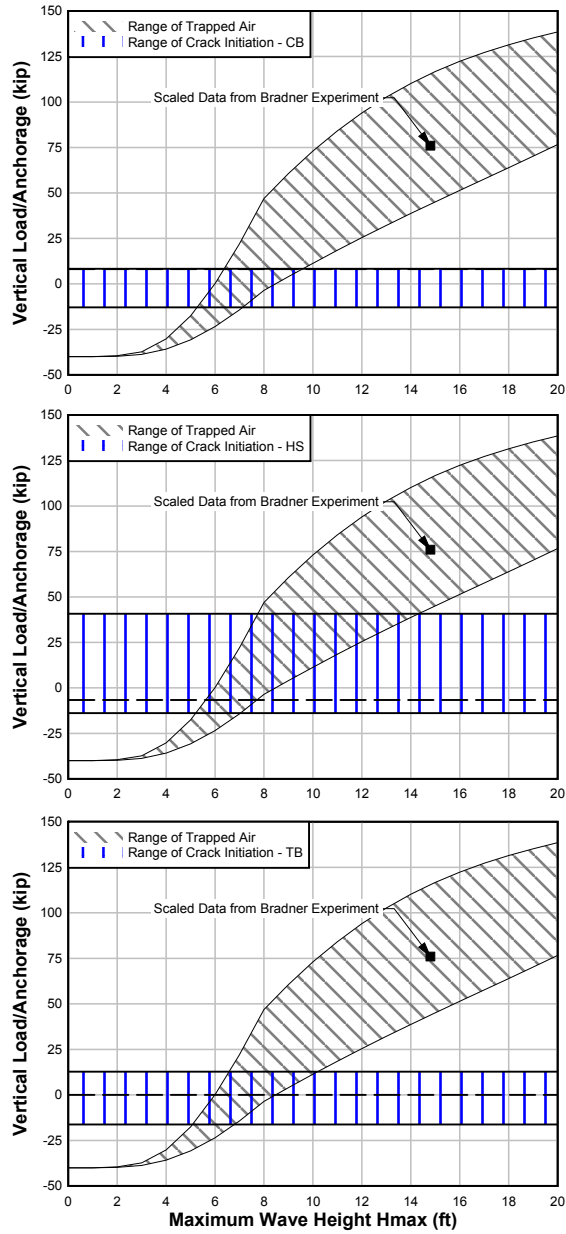


Figure F- 5: AASHTO Vertical Load per Anchorage and Crack Initiation

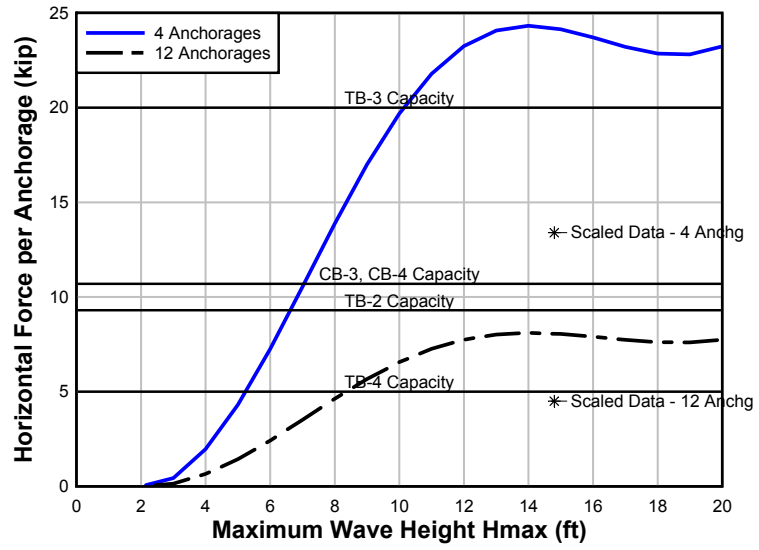


Figure F- 6: AASHTO Horizontal Load per Anchorage and Crack Initiation

Appendix G: Specimen Production

The specimens were fabricated by Knife River in Harrisburg, OR. The specimens were cast on two separate days, with one girder of each anchorage type cast on each day. Cast 1 occurred on August 10, 2009, and was cut down on August 14, 2009. Cast 2 occurred on August 14, 2009, and was cut down on August 17, 2009. Knife River used a three-part steel form, with a continuous bottom soffit and split sides to form the stem and flanges.



Figure G- 1: Knife River Prestressing Bed

The top of the specimens were finished with steel trowels. The strand was jacked using a single block, meaning all strands were pulled to the same jacking force at the same time.

Concrete design targets were 3,500 psi at transfer and 5,000 psi at 28 days. The mix was designed by Knife River engineers to achieve these targets.

Modifications were made to the AASHTO III girders to facilitate testing and to induce a failure at the connection point. The modifications are discussed in the body text. Figure G-2 shows the hairpins, steel loading jig, and bundled #4 steel reinforcing.



Figure G- 2: Reinforcing Modifications to Test Specimens

Figure G- 3 shows the blockouts for the top flange of the AASHTO III section to facilitate loading of the specimens. Square steel tubes were attached to the formwork to maintain the geometry of the steel loading jig.



Figure G- 3: Top Flange Blockouts

Figure G- 4 through Figure G- 6 show the configuration of each different anchorage type in the prestressing beds. Also shown is the steel banding surrounding the prestressing strand.

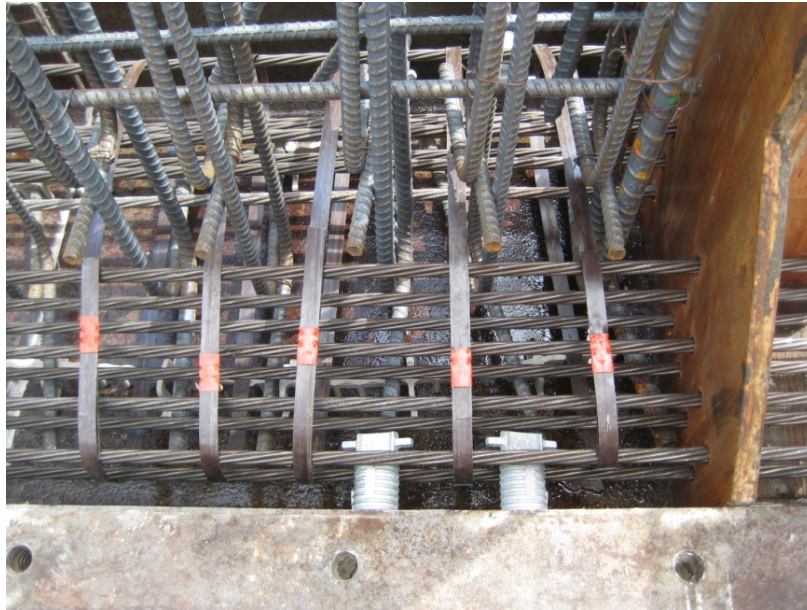


Figure G- 4: Clip Bolt (CB) Anchorage

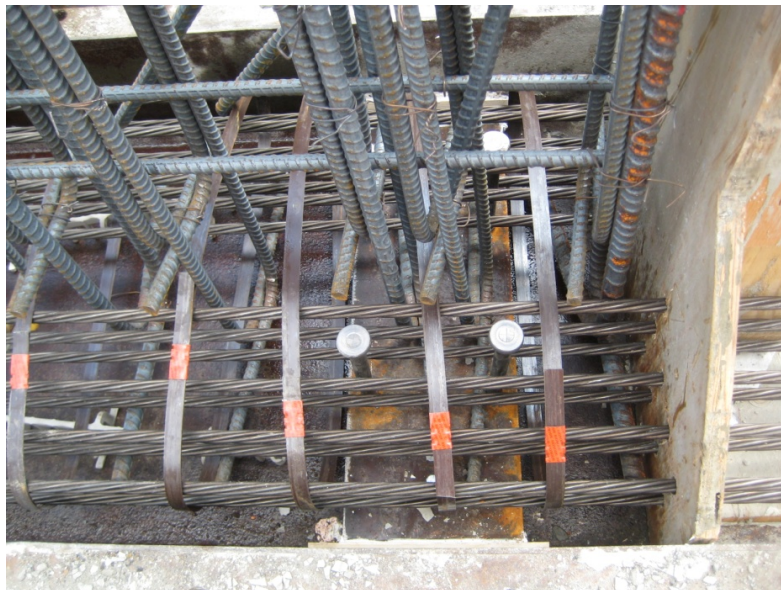


Figure G- 5: Headed Stud (HS) Anchorage



Figure G- 6: Through Bolt (TB) Anchorage

When the concrete reached the specified transfer strength, the strand was cut with an oxy-acetylene torch and the girders were removed from the forms for finishing.



Figure G- 7: Torch Cutting of Prestressing Strand



Figure G- 8: Removal of Specimen from Formwork



P.O. Box 751
Portland, OR 97207

OTREC is dedicated to stimulating and conducting collaborative multi-disciplinary research on multi-modal surface transportation issues, educating a diverse array of current practitioners and future leaders in the transportation field, and encouraging implementation of relevant research results.